Massachusetts Institute of Technology

MONTAN UNIVERSITÄT
WWW.UNILEOBEN.AC.AT

Research project

Investigations of drillability and the borehole stability in crystalline rock formations

Analysis of a deep geothermal power plant situated in an underground mining structure

Stefan Lorenz

(30.09.2015j)

Department of Civil and Environmental Engineering
Massachusetts Institute of Technology

77 Massachusetts Avenue,
Cambridge, MA 02139-4307
Tel.: (617) 253-7101
https://cee.mit.edu

Table of contents

1 Project objectives

Different investigations will be performed to evaluate the potential of a deep geothermal power plant, which is situated in an underground mine structure. The target is to examine the technical and geothermal requirements for the construction of such power plants.

The focus of the investigation is the analysis of drilling a deep borehole from an underground cavern. In a first step the rock mechanical boundary conditions are defined. This will make it possible to determine the drill length and diameter requirements. Also borehole stability and the stress around the borehole will be determine based on a parametric geotechnical analysis.

In this research different borehole geometries, geotechnical conditions and stress regimes will be investigated.

Deep geothermal reservoirs are often linked with unusual stress conditions at depth. The stress regime (orientation and magnitudes of the stress field) is subject to variations with depth and geology. The main objective is to find a way to reduce the stress below the drill bit. This is will make it easier for the drill bit to break the rock. To investigate this issue finite element simulations will be done. The simulations will be done with a model of the borehole using the finite element code ABAQUS. The results of the study will then be included in the conceptual design.

2 Project in general

The aim of the research is to study the technical basis for the construction of a deep geothermal power plant in an existing subsurface mine. The concept intends to make use of conditions with high geothermal gradients, similar those shown in Figure 2-1.

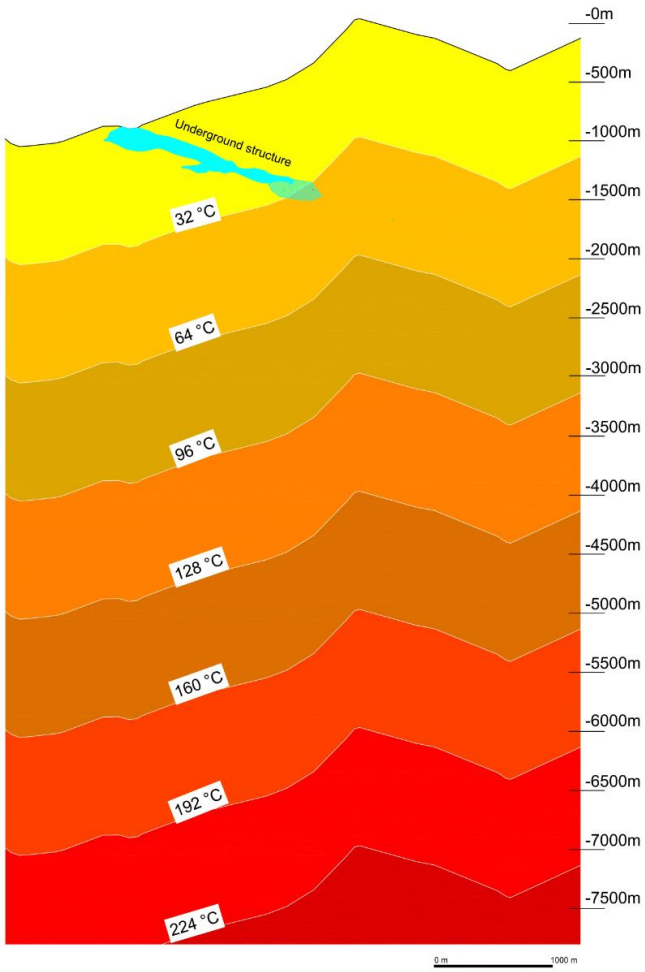

Figure 2-1 geothermal situation

Starting from such underground openings with wells of reduced depth might makeenergy extraction technically more feasible and economical. The innovative aspect is in the use of the already existing rock temperature at this depth (appr. 1000 meters) of about 30°C, considering a geothermal gradient of 3°C per 100 meters to reach a target depth of 5000 meters to achieve a rock temperature of 180°C. This compares to a well depth of 6000m if drilled from the surface. The benefit of this concept is obvious considering in this context the drilling costs, which increase almost exponentially with depth.

In this research special focus is placed on investigations of the basics of deep drilling in crystalline rock for energy extraction. The borehole stability and the stress distribution around the well are calculated depending on different initial stress states. The calculations are also related to innovative drilling concepts. Today drilling wells and developing geothermal reservoirs in deep and hard rocks represent a major challenge for the industry.

3 Project conditions

In this research the technical feasibility of a deep geothermal power plant, based on an Austrian underground project, is being investigated. The location is in the area of the underground mine Breitenau in Styria. The rock overburden in this project is around one thousand meters. In the project crystalline bedrock is expected at depths of about six kilometers. This crystalline rock was tested for relevant geothermal parameters. The existing underground openings allow one to start drilling at that level rather drills from the surface. The geological formations are shown in Figure 5-1.

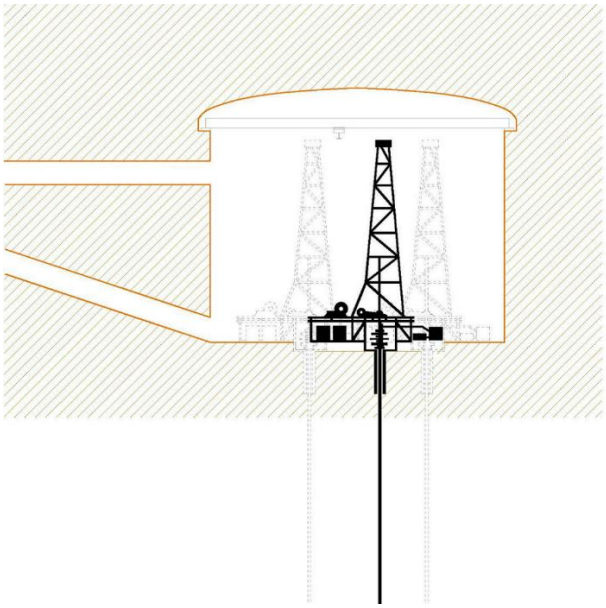

Figure 3-1 drill-rig in underground structure

4 State of the art in field of borehole stability considerations

When creating a well, the surrounding rock and the hole are subject to a variety of effects. The following section describes and summarizes these effects.

4.1 Interaction borehole and formation – stress distribution

Knowledge of the in-situ stress is important for borehole stability analyses.

Mechanical wellbore instability is a result of the interplay between in-situ stresses, mud weight (pressure), pore pressure, wellbore trajectory, and rock properties. A linear-elastic analysis is frequently used for the prediction of the onset of wellbore failure and the optimum mud-weight window required to prevent both hydraulic fracturing of the formation and hole collapse as a result of shear failure. The optimum mud weight must be great enough to prevent high underbalance/blowout and borehole shear failure and low enough to avoid hydraulic fracturing the formation. (G. Li & M. Bai, 2012)

The calculations for the borehole stability are performed in section 6. In this context also estimations about the mud weight are carried out.

4.2 Stress distribution - Mechanical model of a borehole

Underground formations are always in a stressed state, mostly due to overburden and tectonic stresses. When a well is drilled into a formation, stressed solid is removed. The borehole wall is supported by the mud pressure in the hole or not supported at all. Consequently, the mud pressure generally does not equal the in situ formation stresses. This leads to stress redistribution around the well. In cases where the resulting deviatoric stresses are higher than what the formation can support, rock failure will occur.The stress distribution around a circular hole in an infinite plate was published by Kirsch 1898.

The mechanical model of a borehole during a drilling process is shown in Figure 4-1. The horizontal maximum principal stress σ_H and minimum principal stress σ_h are imposed on the formation. The maximum principal stress represents the primary stress p_0 in the formulas 4-1 and 4-2. The equations apply for a vertical borehole along number of the principal stresses. The angle θ is measured relative to the

direction of the major horizontal stress. This means that the shear stresses are zero by an angle of θ=0

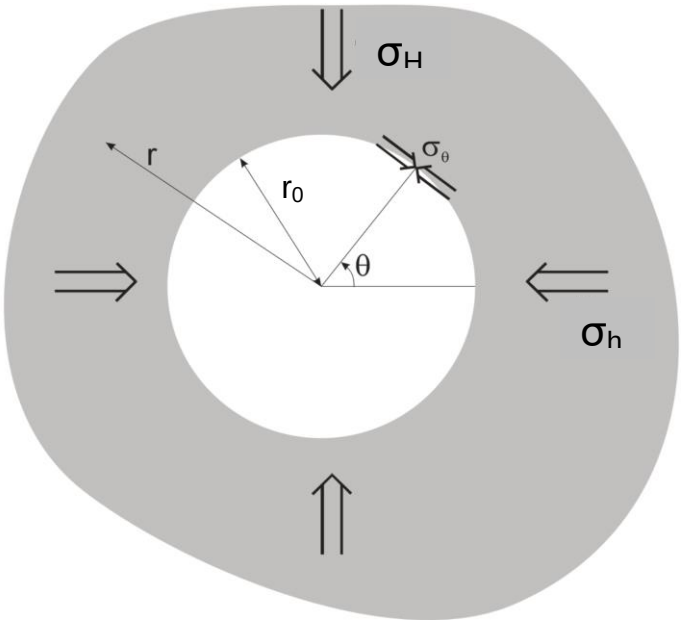

Figure 4-1 Mechanical model of a borehole

$$\sigma_r = p_0\left[\frac{1+k_0}{2}\left(1-\frac{r_0^{\,2}}{r^2}\right)-\frac{1-k_0}{2}\left(1+3\frac{r_0^{\,4}}{r^4}-4\frac{r_0^{\,2}}{r^2}\right)\cos 2\theta\right] \qquad \textbf{4-1}$$

$$\sigma_\theta = p_0\left[\frac{1+k_0}{2}\left(1+\frac{r_0^{\,2}}{r^2}\right)+\frac{1-k_0}{2}\left(1+3\frac{r_0^{\,4}}{r^4}\right)\cos 2\theta\right] \qquad \textbf{4-2}$$

Where: σ_r is the radial stress on the wall rock in MPa, σ_θ is the circumferential stress on of the wall rock in MPa, r is the distance between any point on the borehole wall rock and the center of the borehole in m, r_0 is the radius of the borehole in m, p_0 is the primary stress in MPa, k_0 is the lateral pressure coefficient.

4.2.1 Borehole failure criteria

Large stress deviations occur in the formation close to the borehole when the borehole pressure differs from the formation pressure. If the stress deviation exceeds the strength of the rock, the rock fails. Stress distributions with a plastic material

behavior and Mohr-Coulomb failure criterion were developed by Kastner (1962). If the rock strength is exceeded, by assuming an elasto-plastic material behavior, a "plastic zone" in the formation occurs. In this case, there is a transition from elastic to plastic behavior. The radial stress at the radius where the material behavior changes from elastic to plastic is referred as "critical support expansion pressure" (equation 4-5).

For the derivation of the radius for the change from elastic to plastic behavior we assume a vertical borehole with isotropic horizontal stresses. Within this assumption, the principal stress formulation is:

$$\sigma_\theta = 2\sigma_h - \sigma_r \qquad \textbf{4-3}$$

By assuming that σ_r is the minimum stress and σ_θ the maximum stress, the Mohr-Coulomb Criterion in the elastic zone one the form like equation 4-4, where $k=k_p = \tan^2\beta$ and β is the failure angle.

$$\sigma_\theta = \sigma_{UCS} + k\sigma_r \qquad \textbf{4-4}$$

At the radius of the plastic zone, the intact material yield criteria must be fulfilled, hence by inserting equation 4-3 into 4-4 it results to:

$$\sigma_r(R_p) = p_i^{cr} = \frac{2\sigma_h - \sigma_{UCS}}{k+1} \qquad \textbf{4-5}$$

If the existing support pressure exceeds the critical support pressure, no development of a plastic zone is induced. Would the support pressure further increase and exceed the primary stress state, there would be a compressive stress of the rock. This is the case when the borehole support pressure (mud weight) is greater than the formation pressure.

The following equations show the basis for the derivation of the stress distribution of the plastic zone.

Using the known relationships, the stresses in the elastic zone, and the stresses in the plastic zone can be written as:

stress distribution plastic zone

$$\sigma_t = -\frac{\sigma_{UCS}}{k-1} + k\left(p_i + \frac{\sigma_{UCS}}{k-1}\right)\left(\frac{r}{r_0}\right)^{k-1}$$

$$\sigma_r = -\frac{\sigma_{UCS}}{k-1} + \left(p_i + \frac{\sigma_{UCS}}{k-1}\right)\left(\frac{r}{r_0}\right)^{k-1}$$

stress distribution elastic zone

$$\sigma_t = p_0 + \left(p_0 - p_i^{cr}\right)\left(\frac{r_p}{r}\right)^2$$

$$\sigma_r = p_0 - \left(p_0 - p_i^{cr}\right)\left(\frac{r_p}{r}\right)^2$$

This derivation expects the same rock characteristics in the elastic and plastic zone. Figure 4-2 shows the schematic representation of a stress distribution around a borehole with the development of plastic zone with linear-elastic ideal-plastic material behavior.

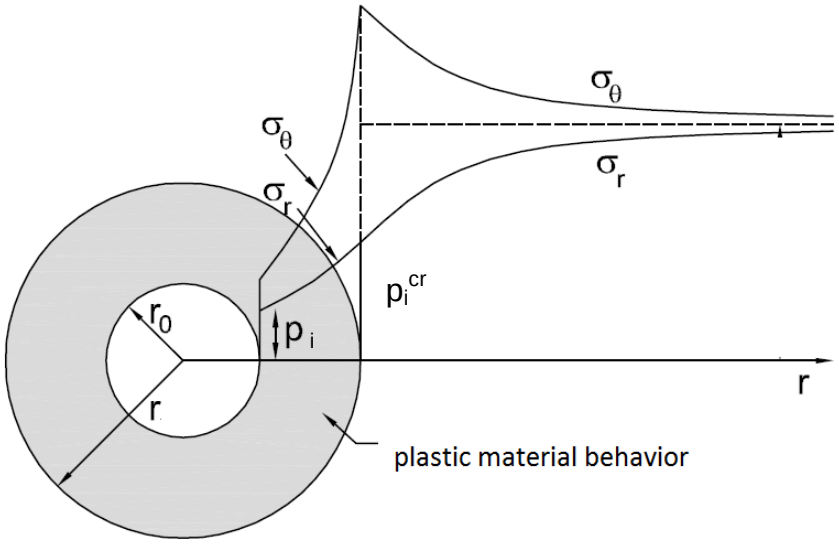

Figure 4-2 Stress arround a borehole wieth a plastic zone (Kolymbas; 1998)

4.3 Drilling process and advanced drilling technology

Current drilling technologies used to drill geothermal wells are mostly identical to those used in the oil and gas Exploration and Production (E&P) industry. The same tools such as PDC bits and mud motors or turbines are used for both applications. Although they are an effective way to drill the well, the time taken to drill 4000 meters in a geothermal well is much longer than for the equivalent E&P well due to the types of formations drilled. The high strength of the crystalline rock makes it difficult to drill, which leads to low penetration rates and short life of the drilling equipment.

Previous work has shown that the cutting performance of drill bits can be improved dramatically when water jets are placed immediately adjacent to the bits. Many studies focus for drilling operation with water jetting techniques in combination with PDC bits. The current status is summarized in section 4.3.1.

4.3.1 Current state of the drill bit for drilling in crystalline rock - jetting

Some research studies describe drilling methods, processes and technologies which allow one to drill hard rock formations faster than currently possible. The advances will not only have an economic and environmental impact but also an impact on emission reduction. Faster drilling will reduce the time taken to complete a project.

One promising technology in this field is the water jetting technique, which is already used to loosen rock in the mining industry. The idea behind it is that the bit rotates for mechanical breakage and removal of cuttings at the bit face. However, the penetration will be mainly due to a water-jet of an (abrasive) jetting fluid. The jets cut slots into the rock, or weakens the rock in front of the bit so that the rock can easily be broken into smaller pieces and removed by the rotating action of the bit.

Since the 1970s, water jet assisted rock breaking has been considered as the most promising assistance rock breaking technology with water jet being introduced to assisting the mechanical tools to break the rock. Previous research (Table 4-1) focuses on the wheather and under which conditions the jets could enhance the overall performance of the mechanical tools.

Other researchers interpret the significant benefits achieved when jets are used to assist the cutting process, are still not fully understood. It is apparent however that one of the main effects of the jets is to facilitate chip removal ahead of the bit during the cutting process (Hood M., 1983). Perhaps, water jets do not much enhance the efficiency of the cutting process itself. The water supports the overall energy use which is needed to remove a given quantity of rock.

Table 4-1 Refernces water jetting

Reference	Rock Types	Pj, MPa	σc, MPa	Se (J/mm3)
Jaeger and Cook (1976)	Hard rock (200 MPa compressive strength)	-	-	10
Pols (1977)	Belgian Limestone, Gres bleu Sandstone, Solnhofen Limestone, Martelange Schist	90	80 - 210	100 - 170
Chadwick - (Maurer 1980)	Berea Sandstone, Salem Limestone, Tennessee Marble, Westerley Granite, Charcoal Granite, Sioux Quartzite, Dresser Basalt	345	-	3-10
Harris and Mellor - (Maurer 1980)	Barre granite	100 - 400	-	100 - 500
Flow (1981)	black granite	350	280	10
O'Hanlon and Madonna (1982)	High Strength: Imberg Sandstone, ande-site, Vermont Granite High strength/impermeable: gneiss, schist, peridotite, quartzite, taconite, basalt, colorado sandstone, Taiwan Siltsone, Extremely high strength: flint	240 240 240	- - -	4 -7 10 -25 80
Vijay et al. (1984)	Muskoka Pink Granite	69	-	10 -50
Agus et al. - (Summers 1995)	granite	125 - 200	-	2,5 - 5
Cable (1993)	cherty and shaley limestone granite	70 -100 70	170 210	10 -30
Kollé et al. (1997)	black granite	350 -240	280	70 -100

4.4 Drilling fluid - mud

When drilling a deep well, the open borehole is first supported by drilling mud inside the hole. However this is not the only purpose of the drilling mud. The used drilling mud has a significant impact on the drilling process and the stability of boreholes. The tasks of drilling mud are:

- transport cuttings to the surface
- cool and lubricate the drill string
- transport gases to the surface
- reduce friction between drill string and borehole wall
- stabilize borehole wall
- prevent inflows from the formation into the borehole

As a result of the very high pump rates of drilling mud, in the range of about 2000 l/min, the erosion of the well is caused by the friction of the fluid with the borehole wall. In addition to the mechanical interaction between fluid and formation a chemical interaction takes place. To improve the stabilizing effect of a drilling fluid different aggregates will be used. Also the chemical interaction with the formation the rheology and density must be taken into account.

To change the drill bit, the entire drill string must be removed. Due to the friction of the drilling fluid between the borehole wall and the drill string, pressure changes, the so called surge (when retracting) and Swab (when replacing) pressures, occur. The calculations of these pressures require accurate knowledge of the rheology of the mud and the geometry of the hole. In general this is only numerically possible. The pressures changes are in the range of about 1 MPa and act as alternating loading.

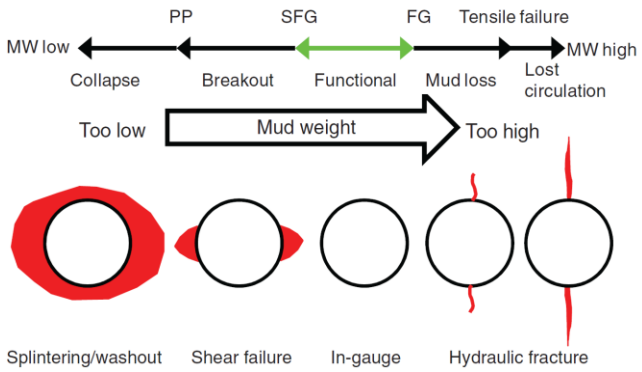

Figure 4-3 Schematic relationship of mud weight an wellbore failures (Zhang et. Al. 2008). MW=mud weigth, PP=pore pressure, SFG=shear failure gradient, FG=fracture gradient

Figure 4-3 illustrates the relationship of mud weight (or mud pressure), pore pressure, and wellbore stability to different borehole failures. When the mud weight, or equivalent circulating density (ECD), is less than the pore pressure, the wellbore experiences splintering failure or spalling. In this case, wellbore washouts or fluid kicks (unwanted flow of fluids from a formation into the wellbore) resulting from underbalanced drilling may occur. In the context of the formation, washouts enlarge the area of the wellbore caused by the removal of formation grains during drilling or circulation. Formation-fluid influx or blowout occurs when the ECD is less than the pore pressure and a permeable formation is encountered. A well may not have fluid kicks in an underbalanced drilling scenario if impermeable formations are penetrated. When the mud weight or ECD is less than the shear-failure gradient (caused by strongly differing horizontal stress states), also called borehole-collapse-pressure gradient, the wellbore experiences shear failure (or wellbore elliptical enlargement, breakout, or collapse). Considerable shear stresses arise from the contrast between the radial and the tangential stress, and the borehole can collapse. Wellbore hydraulic fracturing occurs when mud pressure exceeds the capacity of near-wellbore rock to bear tensile stress and the drilling fluid creates hydraulic fractures. The drilling induced fractures may cause drilling fluid losses and even a total loss of drilling fluid (lost circulation). (Shuling L. e al., 2012)

4.5 Casing

Casing and tubing strings are the main parts of the well construction. All wells drilled for the purpose of oil or gas production and also for heat extraction must be cased with a material with sufficient strength and functionality. To ensure long-term stability of wells strings of steel pipes are installed in the wellbore. By designing the casing the

acting rock pressures must be considered. The effect of a casing has been studied in a model, and will be discussed in section 6.2

5 Laboratory tests

In order to obtain the initial data for calculations and simulations, it was necessary to determine the geological and geotechnical parameters. In the following sections the geological and geotechnical conditions are described.

5.1 Geologie

The most relevant area within a geothermal setting/system is the crystalline layer of rock, since it will act as heat source. Because no direct or indirect exploration of the crystalline zone of the Breitenau mine exists, the layer has been analyzed based on surface outcrops.

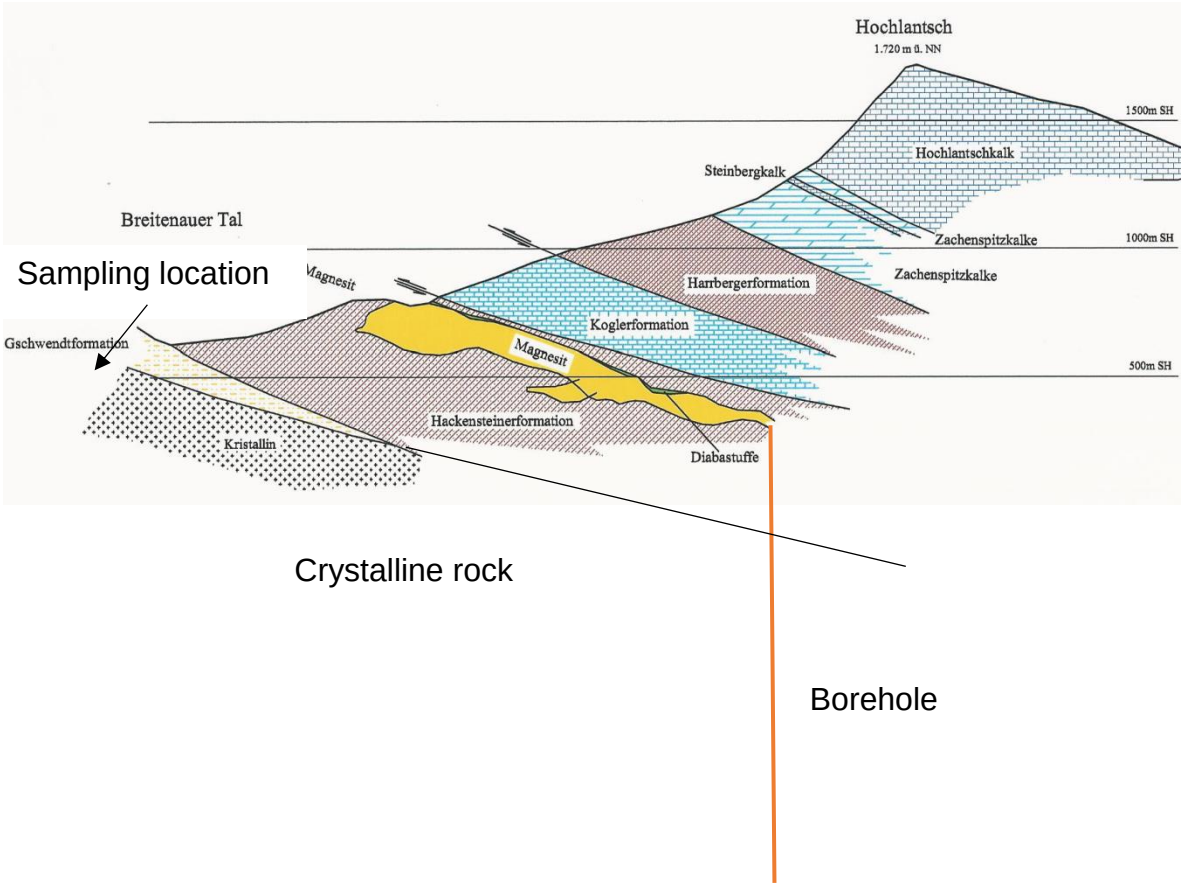

Figure 5-1 geological conditions (Gollner & Zier, 1982)

Investigations show that mostly gneiss, amphibolite and schist exist and in a slate formation. Because of the occurence of biotite and hornblende the rocks have a dark form of appearance. As shown in Figure 5-2, the formations additionally show a pronounced bending.

Figure 5-2: Sample of Amphibolite

XRD	**Amphibolite [%]**
Calcite	nd
Dolomite	nd
Quartz	7,5
Plagioclase	30,9
K Feldspar	nd
Muscovite	nd
Biotite	2,5
Chlorite	nd
Kaolinite	nd
Augite	nd
Amphibole	59,1
Garnet	nd
Apatite	nd
Amorphous	nd
Sum	**100,0**

Amphibolite is a grouping of rocks composed mainly of amphibole and plagioclase feldspars with little or no quartz. It is typically dark-colored and heavy with a weakly foliated or schistose (flaky) structure.

Table 5-1 Mineralogical composition

Mineral	**[Vol. %]**
Quarz	12-16
Plagioklas	36-43
Kalifeldspat	3-4
Amphibol	12-19
Biotit	15-24

5.2 Rock mechanical properties

Standard laboratory test (UCS, Young's modulus, brazilian test) the mechanical properties were performed. Average values are listed in Table 5-2 below.

Table 5-2 geotechnical properties

UCS			**E_s**	**Tensile splitting (Brazilian)strength**		
Mean value	**Min**	**Max**		**Mean value**	**Min**	**Max**
[Mpa]	[Mpa]	[Mpa]	[Gpa]	[Mpa]	[Mpa]	[Mpa]
169	92	279	43	15	7	26

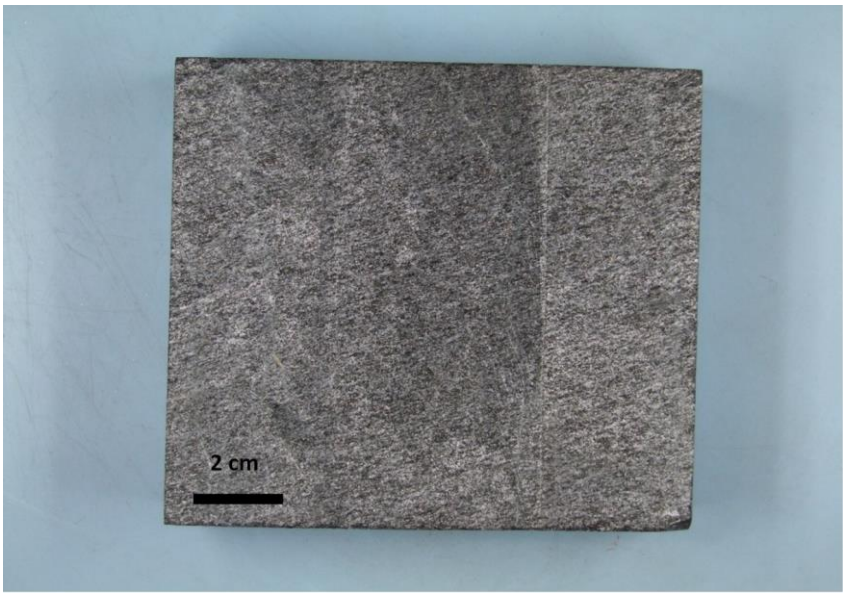

Figure 5-3 Testing sample Amphibolite

Additional data were provided by the mining company (RHI)

Specific weight = 29.0 kN/m³

Poisson ratio = 0.35

Friction angle = 27.0°

6 Analysis

6.1 Stress distribution around the borehole

The mechanical relations on while the holes calculations as described in sequence/section 2.2.

The stress distribution is calculated for the highest layered overburden at the bottom of the borehole. Further the stresses of the bore hole in the area of the next larger diameter of the casing are calculated.

For a borehole length of 5000 m the overburden is 6000 m. The vertical stress is estimated ..rock weight (29 kN/m³) and the overburden depth of the chosen final diameter of the borehole is 18 cm (casing 3,5 inch). Also the stresses at an overburden of 3500 m and a provided diameter of 25 cm (9,63 inch) were calculated. The evaluation follows the formulas in section 4.2. The calculations are done for the worst case scenario, which means that there is no drill fluid (mud) in the hole and thus the support pressure p_w is zero.

6.1.1 Calculation at 6000 m depth

Overburden	6000 [m]
Borehole diameter	0.18 [m]
Support pressure pw	0 [MPa]
Friction angle	27 [°]
Specific weight γ	29 [kN/m³]
Young's modulus E	43000 [MPa]
Poison ratio v	0.35 [-]

Calculation of the σ_{UCS} with equation 2.5:

Uniaxial compressive strength σ_{UCS} 1000 [KN/m²]

From the context of equation 2.4 calculated the k:

Earth pressure coefficient k 2.662 [-]

The plastic radius is 1.89 m calculated with equation 2.5. The critical support pressure in this case is 94.73 MPa. Figure 6-1 shows the stress distribution around the bore hole without support pressure.

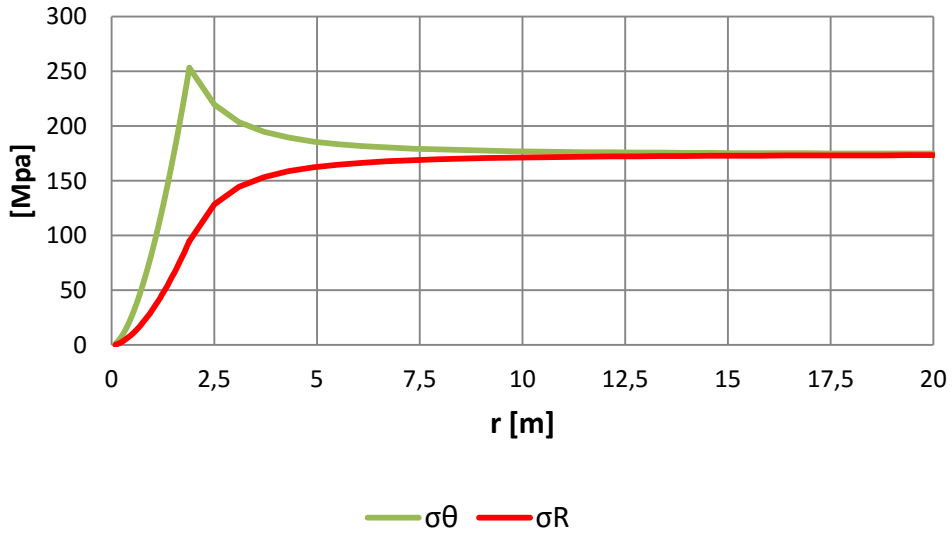

Figure 6-1 stress distribtion at the borehole bottom

6.1.2 Calculaton at 3500 m depth

Input parameters casing extension:

Overburden	3500 [m]
Borehole diameter	0.25 [m]
Support pressure pw	0 [MPa]
Friction angle	27 [°]
Specific weight γ	29 [kN/m³]
Young's modulus E	43000 [MPa]
Poison ratio v	0.35 [-]

The plastic radius is 1.90 m calculated with equation 2.5. The critical support pressure in this case 55.15 MPa. Figure 6-1 shows the stress distribution of the bore hole without support pressure.

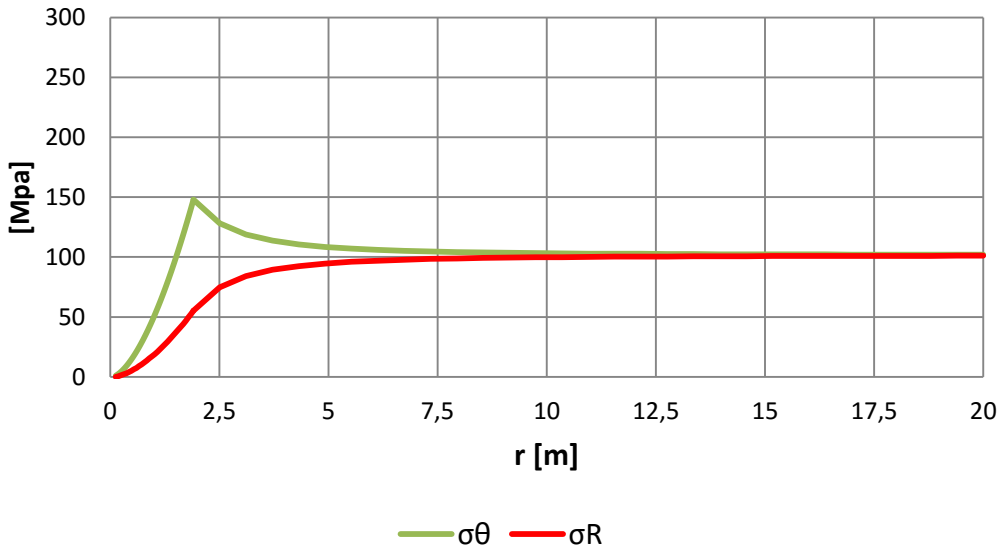

Figure 6-2 stress distribution casing extension

6.2 Casing design

The casing serves several important functions in drilling and completing a well. It prevents a collapse of the borehole during drilling and hydraulically isolates the wellbore fluids from the subsurface formations and formation fluids. It minimizes damage of both the subsurface environment during the drilling process and the well exposed to a hostile subsurface environment. It provides a high-strength flow pipe for the drilling fluid and, with the blowout preventers (BOP), permits the safe control of formation pressure. Selective perforation of properly cemented casing also permits specific interaction with a given formation of interest. (Adam T. et al, 1986)

The casing process begins with the specification of the surface and the bottom hole well size of the production casing that will be used. The number of casing strings and the type of the subsurface artificial lift system equipment that is placed in the well and geothermal system considerations determine the minimum inner diameter (ID) of the producing casing. For the following heat transfer simulations an outer diameter of 7 inches was calculated for the bottom hole well. The selection of the number of casing strings and their respective setting depths are based on the consideration of the pore pressure and fracture pressure gradients of the formation to be penetrated.

The installation depths of the individual pipe strings (casings) are determined on the basis of the mud weight window (MWW). The following assumptions were made:

- For the first calculation the density of the rock is assumed to be constant with 2700 kg/m^3
- and the second one was calculated with 3150kg/m^3. The first two numbers represent the minimum and maximum of amphibolite (compare section 5.2).
- Pore pressure is derived from the water density and hydraulic head.

The mud weight window represents the pore pressure, mud weight and frac pressure over depth. The weight of the drilling fluid should be more than 3% of the pore pressure in the ideal case, otherwise the pore liquid would flow into the well, where it can lead to complications during the drilling process (Bourgoyne A.T.Jr et.al;1986).

The mud weight window shows that theoretically only one casing is needed from the starting point of drilling down to the end depth. However, a three-part casing is chosen due to safety reasons and for reducing the weight that is loaded onto the drilling rig. The outer diameter of the production casing is set to 7 inches. (Bauer et al., 2014) The casing diameters are given in inches and are standardized by the API (American Petroleum Institute). (API Bulletin, 1999) On the basis of a fit diagram (Figure 6-6) most outer diameters are determined.

The pressure inside the borehole must always be in the range between the pore pressure and the frac pressure of the rock. For the frac pressure a safety factor of 3 % is taken into account. Based on the described conditions, the individual casing strings are determined by the MWW.

Vertical stress is assumed to be a principal stress, and is usually considered to be solely due to the weight of the overburden. That is:

$$\sigma'_v = \rho * g * h \qquad \textbf{6-1}$$

In the calculation it is assumed that isotropically and tectonically relaxed areas are given, so the minimum and maximum horizontal stresses are the same. The pore pressure is calculated as hydrostatic pressure by the overburden.

$$p_f = \rho_w * g * h \qquad \textbf{6-2}$$

As discussed previously, borehole fracturing will occur if the well pressure rises above the fracture initiation pressure, p_{frac}. Thus, the upper bound for mud weight window can be calculated. Estimations of formations fracture pressure before the installation of the casing in the well are based on empirical correlations. The formation fracture pressure is affected greatly by the formation pore pressure. The commonly used fracture pressure equations and correlations include the Hubbert and Willis equation. The minimum well bore pressure required to extend an existing fracture was given as the pressure needed to overcome the minimum principal stress (Hubbert & Miller, 1957):

$$p_{frac} = \sigma_{min} + p_f \qquad \textbf{6-3}$$

The mud weight window in Figure 6-3 shows that in theory only a single casing string of drilling location is required until the final depth.

For the calculation following parameters and equations are used:

- Density: 2700 kg/m³ - 3150 kg/m³
- Poisson's ratio: 0.35
- Density pore fluid (water): 1000 kg/m³

σ_{v1}	vertical stress (density 2700 kg/m3)
σ_{v2}	vertical stress (density 3150 kg/m3)
p_p	pore pressure
p_{frac1}	fracture pressure (density 2700 kg/m3)
p_{frac2}	fracture pressure (density 3150 kg/m3)

Depth [m]	σ_{v1} [bar]	σ_{v2} [bar]	p_p [bar]	p_p [kg/m^3]	p_{frac1} [bar]	p_{frac1} [kg/m^3]	p_{frac2} [bar]	p_{frac2} [kg/m^3]
0	0	0	0	-	0	-	0	-
500	132	155	49	1000	94	1915	106	2158
1000	265	309	98	1000	188	1915	212	2158
1500	397	464	147	1000	282	1915	318	2158
2000	530	618	196	1000	376	1915	423	2158
2500	662	773	245	1000	470	1915	529	2158
3000	795	927	294	1000	564	1915	635	2158
3500	927	1082	343	1000	658	1915	741	2158
4000	1059	1236	392	1000	752	1915	847	2158
4500	1192	1391	441	1000	846	1915	953	2158
5000	1324	1545	491	1000	939	1915	1058	2158
5500	1457	1700	540	1000	1033	1915	1164	2158
6000	1589	1854	589	1000	1127	1915	1270	2158

Table 6-1 Calculation mud weight window

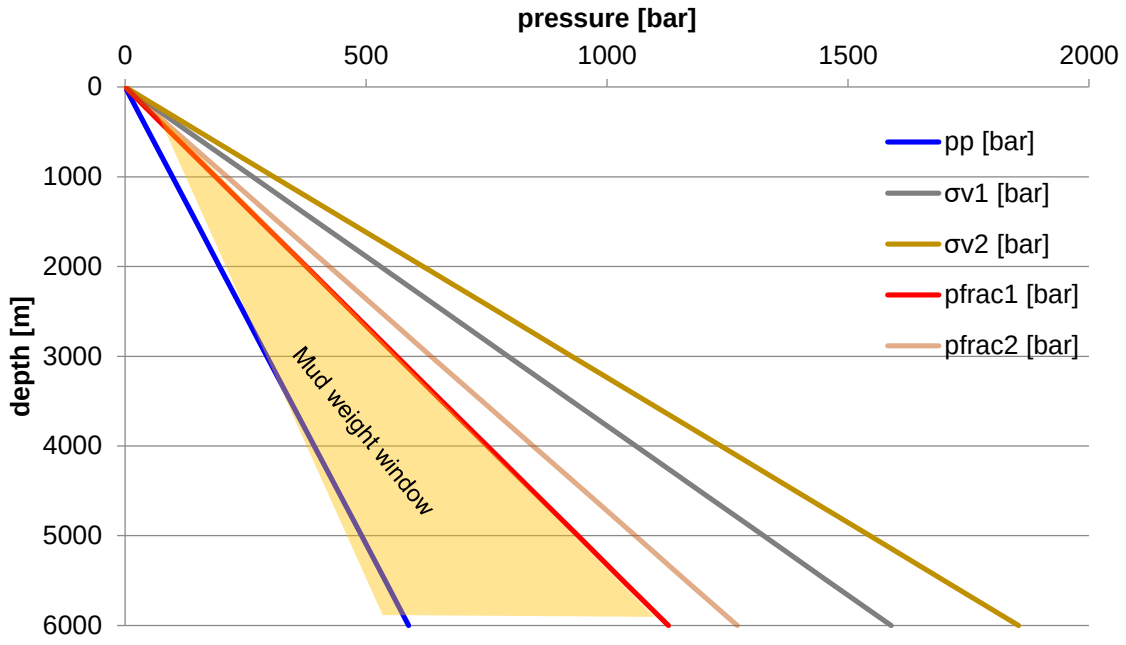

Figure 6-3 Mud weigth window

6.2.1 Casing strings

The size of the casing strings is controlled by the necessary inner diameter of the production string and the number of intermediate casing strings, which are required to reach the aimed depth. The surface casing prevents a break-in of unconsolidated weaker formations under the drill rig. The surface casing setting depths depend on the strength of the formations below. In this calculation the considered length is 300 m.

When abnormal formation pore pressures are present in the deeper formations of a well, an intermediate casing is needed to protect formations below the surface casing from the pressures created by the required high drilling mud density. Similar, when normal pore pressures are found below sections and are having an abnormal pore pressure, an additional intermediate casing permits lowering the mud density to drill deeper formations. According to the current state of knowledge, no intermediate casing is necessary, but because of safety reasons one intermediate casing is considered in the calculations starting at a depth of 2500 m.

The production casing is the liner which reaches the planed bottom of the borehole. The diameter of the production casing specifies all the other diameters of the casing strings above.

The API provides tables of commonly used bit sizes that will pass through API casings for the estimation of the casing diameters. The selection of the casings was made by API Bulletin 5C2. This document describes the characteristics of the standard casings and tabulated them. (API Bulletin 5C2, 1999)

Basically, two fits are possible, a standard-fit and a fit with a reduced distance between the casings (low clearance). The low clearance scenario represents a disadvantage with any additionally required casings. There would be too little room for a further casing and the end diameter would need to be reduced. However, the use of a further casing can only be evaluated during drilling and with new geological findings. The low volume of the annulus and therefore the more compact casing allows more efficient heat transport. The surface casing extends to a depth of 300 m below the starting point of drilling (1225 m below ground) and it is used to stabilize the rock on the first meters of drilling. The intermediate casing reaches a length of 2600 m with a depth of 3525 m. The production casing is anchored into the intermediate casing as a liner. The production liner with a length of 2500 m reaches a final depth of 5925 m and overlays with the intermediate casing for 100 m. The overlay is needed for the installation (Figure 6-4).

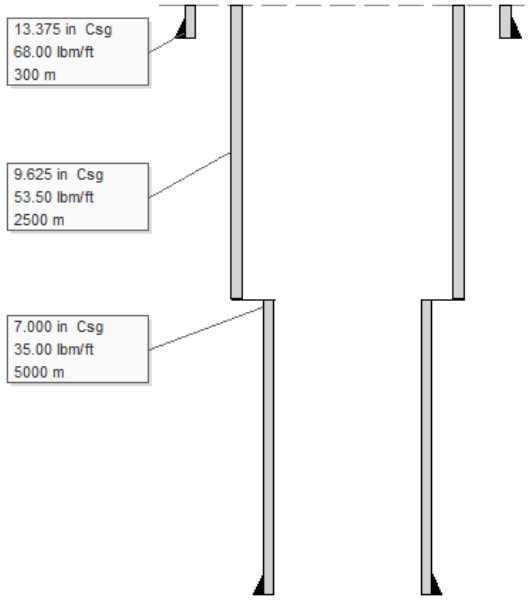

Figure 6-4 Casing, standard clearance, Casing A

Using the API tables the different outer diameters (OD) can be determined. In this calculation the "low clearance" version is selected. In this the distance between the

outer diameter of the inner pipe and the inner diameter of the outer tube is reduced to a minimum compared to the standard version.

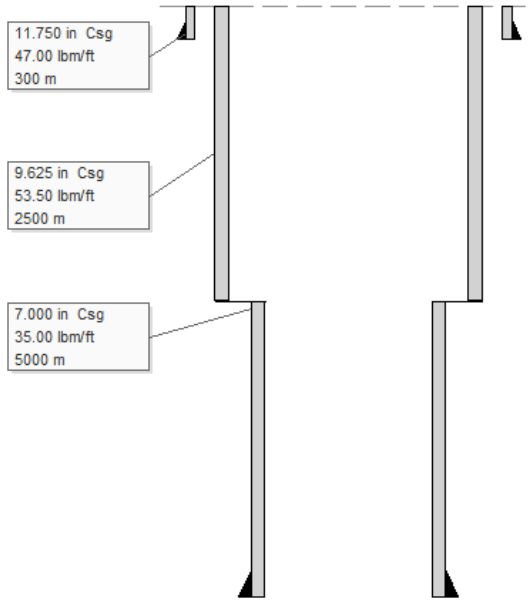

Figure 6-5 Casing, low clearance, Casing B

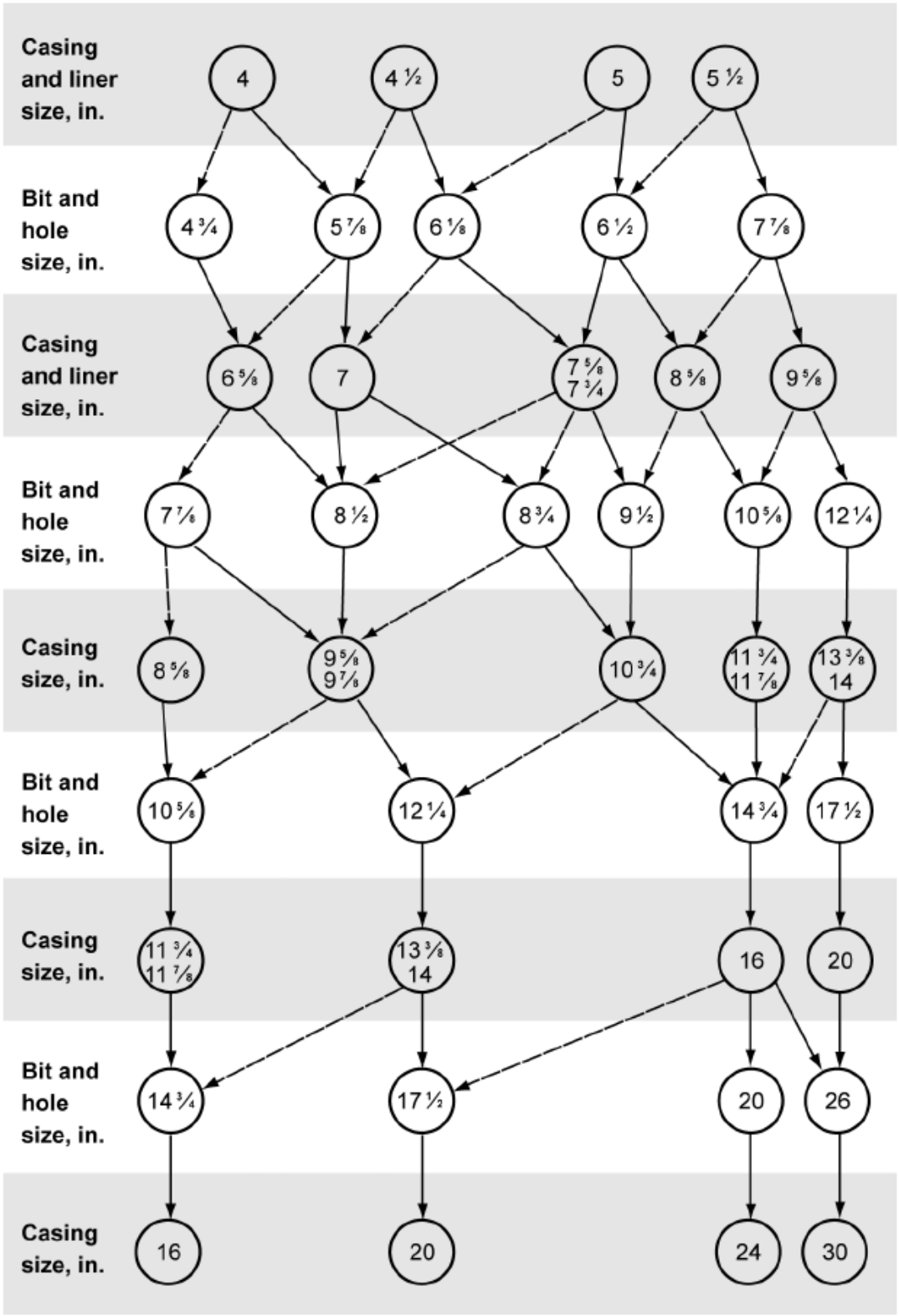

Figure 6-6 Fit diagram: bit and outer diameter of casing (Lake & Mitchel, 2006) Standard-fits (full line) and tight fits (dashed) are represented

Due to the low clearance between the pipes a more economical relationship between surface and production casing diameters is given.

The following Table 6-2 summarizes the single casings with their outer diameter, depth and length. Regardless of that a conductor casing which supports the rock during the drilling of the first 60 m must be realized. In this area the rock is weakened by the excavation of the cavern and for safety reasons needs to be supported. The pore pressure at the starting point of drilling can be particularly difficult. Theoretically, up to 91 bar hydrostatic pressure can occur on the rock, because the starting point of drilling is situated at a depth of 925 m below surface.

Table 6-2 Casings for a 7" production pipe

Casing	**OD [in]**	**from [m]**	**to [m]**	**from [m]**
Surface Casing	11 3/4"	925	1225	300
Intermediate Casing	9 5/8"	925	3425	2500
Production Liner	7"	3325	5925	2600
			total length	**5000**

6.2.2 Planning of well casing

When choosing the casing a number of criteria must be taken into account. The calculation is based on uniaxial stress scenarios for each of the three casings. Burst, collapse and axial stress of each casing are taken into account. For each, the surface, the intermediate and the production casing, an internal and external pressure profile exist. These profiles reflect the stresses inside the casing and also the external stress on the casing. Regarding the tensile load it needs to be considered that the maximum hook load of the drill rig may not be exceeded, as well as the resistance to tension of the casing and bolted joints. This results in a limit for the weight of the casings. In terms of the costs a compromise between the steel quality used and the weight per meter length is required. Higher quality steel and higher weight lead to a higher financial cost. The necessary requirements for the well casing must never be neglected in favor of the costs.

The following table shows the assumptions and at the same time the calculation basis for each unfavorable situation, which may occur in each casing. It needs to be noted, that the unfavorable situation represents a case, which can occur under special circumstances during drilling or later during operation of the drilling. The probability of occurrence is statistically rather low, which is why the planning at the same time represents the worst case. The “Leitfaden zur Futterrohrberechnung” from the „Wirtschaftsverband Erdöl- und Erdgasgewinnung e.V.“ forms the basis for the

technical design and calculation. (Wirtschaftsverband Erdöl-und Erdgasgewinnung, 2006)

For dimensioning the casings following verification calculation have to be considered (Figure 6-7):

- Axial tension - Tensile stress due to the weight of string is highest at top
- Burst pressure - Assume full reservoir pressure all along the wellbore
- Collapse pressure - Hydrostatic pressure increases with depth

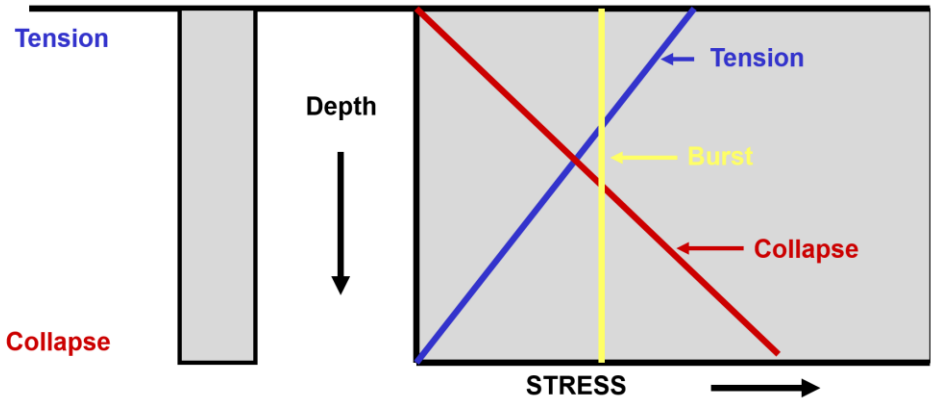

Figure 6-7 Casing design

Therefore the load conditions, which act in depth on the casing, must be accepted. In the following calculation a worst and a realistic case were considered.

Well Information		Depth @ shoe		EMW @ shoe		
Type	Diameter	TVD	MD	Pore EMW	Mud EMW	Frac EMW
	[in]	[m]	[m]	[kg/m^3]	[kg/m^3]	[kg/m^3]
Conductor	-	0	0	-	-	-
Surface	11 3/4	1225	1225	1000	1030	1915
Intermediate	9 5/8	3425	3425	1000	1030	1915
Production	7	5925	5925	1000	1030	1915

Additional Data		
Parameter	Value	Unit
Steel density	7850	kg/m3
Gas density	0	kg/m3

Design Factors	
Collapse	1,125
Burst	1,100
Tension	1,800

The collapse design load is calculated by a hydrostatic mud load (which simultaneously represents the formation pressure) at the bottom of the analyzed casing with consideration of the corresponding safety factor.

The burst design loads are calculated using the pore pressure at the depth where the next casing string is built into the borehole (see Figure 6-4). Because only after installing the next string the pressure conditions change.

The difference between the worst and the realistic case is the basic approach of the burst design loads (external pressure). In the first case hydraulic loads (pore pressure) were used for the calculations and for the second case the frac pressures were taken.

For the detection of tension loads the weight of the casing of the string is compared with the yielding strength.

All specific resistances can be seen in the spreadsheets of the API.

6.2.2.1 Burst load

Burst loads are calculated by superposed load scenarios. For each borehole section different internal and external pressure profiles exist. To obtain the resulting burst load the external pressure profile needs to be subtracted from the internal pressure profile. There is a high probability that burst loads occur at the wellhead respectively at the liner connection.

6.2.2.2 Maximum possible shut in pressure

This load case only appears during drilling. It is assumed that a gas inflow from the next drilling section occurs. The entire hole is filled with gas. The resulting maximum head pressure is calculated from the fracture pressure at the casing shoe minus the gas column in the borehole.

$$p_i = \rho_{frac} \cdot 9.81 \cdot TVD_{casing\ shoe} - \rho_{gas} \cdot TVD_{casing\ shoe}$$

The maximum possible shut in pressure is used for the calculation of the internal profile for surface casing.

6.2.2.3 Head pressure 40% of the invert pressure

This load case only occurs during drilling. An embedded gas kick rises to the borehole head above the drilling fluid level. The pressure that the gas column applies against the borehole head is 40% of the hydrostatic pressure of the subjacent fluid column

$$p_i = 0.4 \cdot \rho_{drilling\ fluid} \cdot 9.81 \cdot TVD_{final\ depth}$$

The internal profile of the intermediate casing is calculated on the basis of this load case.

6.2.2.4 Full gas column

Full gas column occurs during drilling or production phase. The hole is shut in and is filled with gas from the casing shoe up to the borehole head.

$$p_i = \rho_{formation} \cdot 9.81 \cdot TVD_{casing\ shoe} - \rho_{gas} \cdot TVD_{casing\ shoe}$$

The full gas column is basis for the calculation of the internal pressure profile of the production casing.

6.2.2.5 Collapse loads

Same as burst loads, the collapse load consists of the internal and external pressure load. The internal profile is subtracted from the external profile so that the resulting force acts inwards.

6.2.2.6 Interior partially empty

This scenario can occur during drilling when the drilling fluid flows off into a permeable zone. The height of the emerging fluid column is obtained by adjusting a

balance between the hydrostatic pressure of the fluid column and the formation pressure.

$$TVD_{drilling\ fluid} = TVD_{final\ depth} - \frac{\rho_{formation} \cdot 9.81 \cdot TVD_{formation}}{\rho_{drilling\ fluid} \cdot 9.81}$$

$$p_i = p_{atm} + \rho_{drillling\ fluid} \cdot 9.81 \cdot (TVD_{casing\ shoe} - TVD_{drilling\ fluid})$$

The load case interior partially empty is basis for the internal pressure profile of the surface and intermediate casing.

6.2.2.7 Interior empty

The load case only occurs during the subsequent operation. The borehole can be completely emptied by unintentional empty transport or in the course of testing. The internal pressure equates the atmospheric pressure of 1 bar.

6.2.2.8 External pressure profile

For the external pressure profile for all burst and collapse loads only one scenario needs to be considered. Basis for this scenario is a hydrostatic fluid column which acts from the outside over the entire borehole length on the casing.

$$p_a = \rho_{drilling\ fluid} \cdot 9.81 \cdot TVD_n$$

6.2.3 Casing selection

The casings were selected on the basis of API Bulletin 5C2. In this document the characteristic properties of the standardised casings are tabulated. (API Bulletin, 1999) The calculations carried out for case A (normal clearance) and case B (low clearance). The table for the calculations for case A are included in Appendix A. The table below shows the calculations for case B. Table 6-3 summarized the selected casings for both variants.

	Section	Quality	Outer diameter	Weight per meter	Inner diameter
CaseA	Surface casing	J-55	13 3/8	68	12,415
	Intermediate casing	S-95	9 5/8	53,5	8,535
	Production casing	L-80	7	35	6,004
Case B	Surface casing	J-55	11 3/4	47	11,000
	Intermediate casing	S-95	9 5/8	53,5	8,535
	Production casing	L-80	7	35	6,004

Table 6-3: Summary of selected casings for case A and B

The assumptions and also calculation principles for the load situations, which may occur in each casing, are considered in the following calculations. The technical design and calculation based on the book "Applied Drilling Engineering" performed. (Burgoyne A.T.Jr et al, 1986)

6.2.4 Tubing design

The tubing serves the productions efficiency and supports the circulation of the heat-storing medium. Water, in this case the medium, is pumped along the surface of the with a specified temperature T1 into the circle space between the bore hole casing and the tubing. Because of the injection pressure and the gravity the medium is moving into the direction of the bottom of the bore hole depth und therefor along the rising geothermal gradient. At the bottom of the bore hole depth the temperature T2 is reached. The medium there entries the production casings, which leads the water back to the surface.

Due to an adequate selection of the material the heat transfer between the inner and outer surface of the tubing can be minimized, in order to reach little heat losses until the exit at the surface. That is the target of such a completion. Especially the isolation through polymeric layers or the technical design of the production casing as a double casing with a vacuum insulation are popular to be used.

The following materials are used as tubing in a deep geothermal thermo-well:

- stainless steel - chrome, nickel, molybdenum in different percentages as alloy elements, corrosion resistant

- re-lined tubing - stainless steel, which at the inner side is thermally insulated with a polymer
- GRP - glass reinforced plastic
- double casing with a vacuum insulation

Because of the appearing loads, as seen at the bore hole casings, the burst, the collapse and the tension loads have to be standardly considered. For the choice of the adequate tubing the American Petroleum Institute published the according guidelines API 5CT. For the use of a riser in a geothermal drilling there are no special requirements but the thermal conductivity of the chosen material. Therefor there is no need of a calculation of the technical parameters in later steps. The tubing for both casing cases (Standard, low clearance) is shown in Figure 6-8 and Figure 6-9.

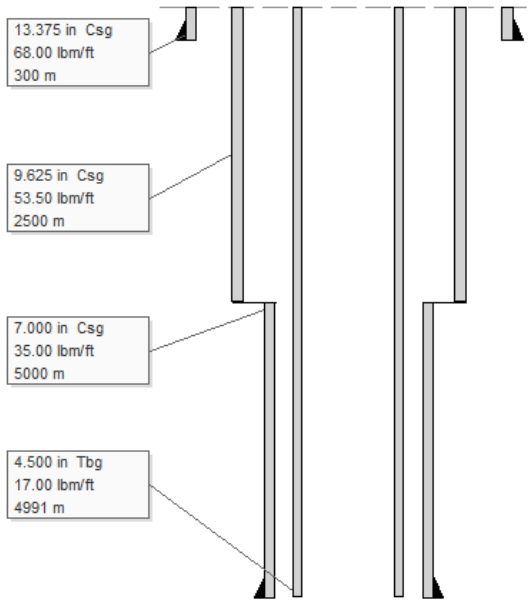

Figure 6-8 Tubing, standard clearance, Casing A

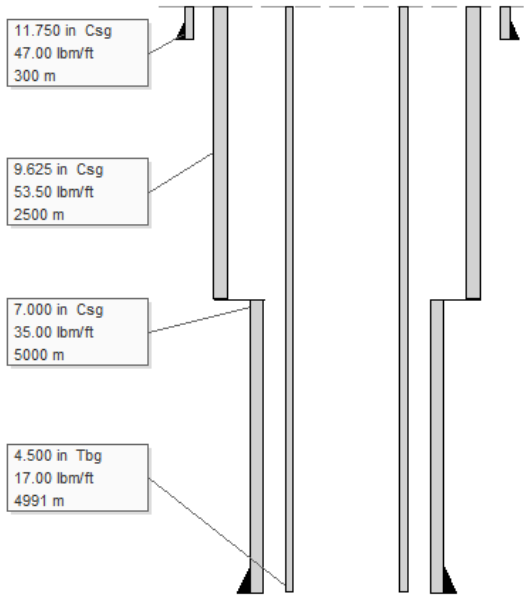

Figure 6-9 Tubing, low clearance, Casing B

Casing Ratings, Worst Case kick from next section @ surface, intermediate / leaky tubing @ production						
Section	**Surface**		**Intermediate**		**Production**	
	[bar]	**[psi]**	**[bar]**	**[psi]**	**[bar]**	**[psi]**
Hydrostatic mud	124	1795	346	5019	599	8683
Collapse design load	139	2020	389	5647	674	9769
Burst design load	370	5360	639	9273	639	9273
Select Casing						
Quality	**L-80**	**11 3/4" 60lb/ft**	**T-95**	**9 5/8" 53.5 lb/ft**	**T-95**	**7" 35 lb/ft**
OD	11 3/4	in	9 5/8	in	7	in
ID	10,772	in	8,535	in	6,004	in
Weight	89,29	kg/m	79,62	kg/m	52,09	kg/m
Coupling	STC		LTC		LTC	
Collapse resistance	3180	psi	7340	psi	11650	psi
	219	bar	506	bar	803	bar
Burst resistance	5830	psi	9410	psi	10970	psi
	402	bar	649	bar	756	bar
Yield Strength	913	1000 lbs	1220	1000 lbs	853	1000 lbs
	4061	kN	5427	kN	3794	kN
Design on Collapse						
Load	139	bar	389	bar	674	bar
Back load	0	bar	0	bar	0	bar
Safety Factor	**1,57**		**1,30**		**1,19**	
Design on Burst						
Load	336	bar	581	bar	581	bar
Back load	0	bar	0	bar	0	bar
Safety Factor	**1,20**		**1,12**		**1,30**	
Design on Tension						
Load	109382	kg	272691	kg	135425	kg
BF	1,000	(in air)	1,000	(in air)	1,000	(in air)
Load*F	109382	kg	272691	kg	135 425	kg
Safety Factor	**3,78**		**2,03**		**2,86**	

Table 6-4 Casing calculation, worst case

Casing Ratings, Realistic Case kick from next section @ surface, intermediate / leaky tubing @ production						
Section	**Surface**		**Intermediate**		**Production**	
	[bar]	**[psi]**	**[bar]**	**[psi]**	**[bar]**	**[psi]**
Hydrostatic mud	124	1795	346	5019	599	8683
Collapse design load	139	2020	389	5647	674	9769
Burst design load	253	3672	708	10267	639	9273
Select Casing						
Quality	**J-55**	**11 3/4" 60 lb/ft**	**S-95**	**9 5/8" 53.5 lb/ft**	**T-95**	**7" 35 lb/ft**
OD	11 3/4	in	9 5/8	in	7	in
ID	10,772	in	8,535	in	6,004	in
Weight	89,29	kg/m	79,62	kg/m	52,09	kg/m
Coupling	STC		LTC		LTC	
Collapse resistance	2660	psi	8850	psi	11650	psi
	183	bar	610	bar	803	bar
Burst resistance	4010	psi	9410	psi	10970	psi
	276	bar	649	bar	756	bar
Yield Strength	649	1000 lbs	1235	1000 lbs	853	1000 lbs
	2887	kN	5493	kN	3794	kN
Design on Collapse						
Load	139	bar	389	bar	674	bar
Back load	0	bar	0	bar	0	bar
Safety Factor	**1,32**		**1,57**		**1,19**	
Design on Burst						
Load	230	bar	644	bar	581	bar
Back load	0	bar	0	bar	0	bar
Safety Factor	**1,20**		**1,01**		**1,30**	
Design on Tension						
Load	109382	kg	272 691	kg	135425	kg
BF	0,869		0,869		0,869	
Load*F	95030	kg	236911	kg	117656	kg
Safety Factor	**3,10**		**2,36**		**3,29**	

Table 6-5 Casing calculation realistic case

7 Numerical simulation

Like described in chapter 6.2 the borehole is subjected to many influences. Since no concluded theory of all considered processes can be used, a numerical procedure has to be chosen for the analysis of the participating processes. Following numerical calculations with the procedure of the finite elements method are presented. Here, the software ABAQUS in the version 6.13 has been used.

In order to limit the numerical computation effort and therefore enabling the numerical calculations of the borehole stability, a two dimensional model with a vertical borehole in the middle is calculated. The numerical model consists of a layer of CPE elements. The radius of the elements is decreasing inwards in order to map the stress gradient at the borehole correctly. This results in 2235 elements for a simplified model (Figure 7-1). As borehole diameter 7’’(case B) were chosen, in accordance with the radius r of 177.8 mm. So that the outer edge of the model is located far enough from the borehole and therefore no impact on the secondary stress field is resulting. The size of the model with an edge length of 50 cm is chosen. This value was derived from test calculations.

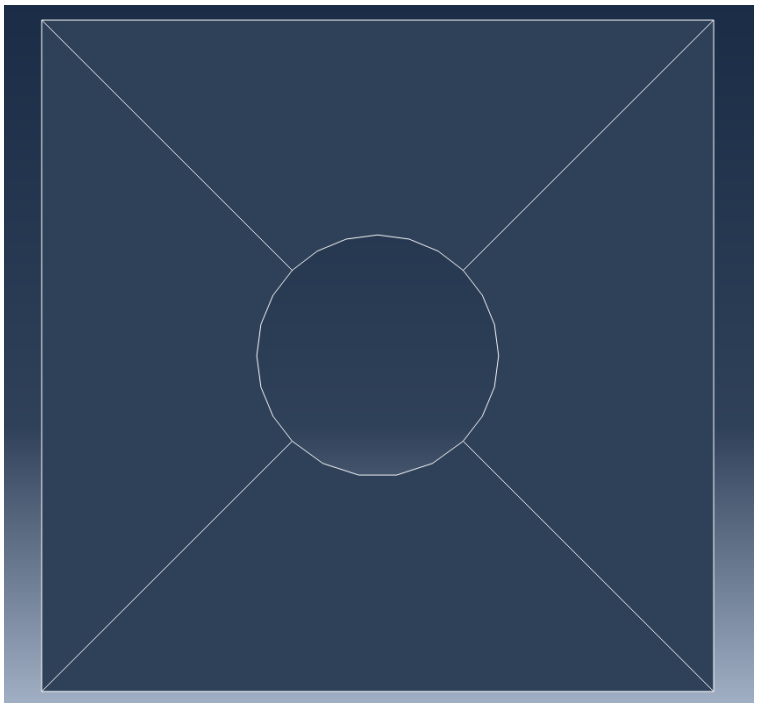

Figure 7-1 Numerical model

The mechanical boundary conditions were chosen, as shown in Figure 7-2. The degrees of freedom of translation were solved with boundary conditions.

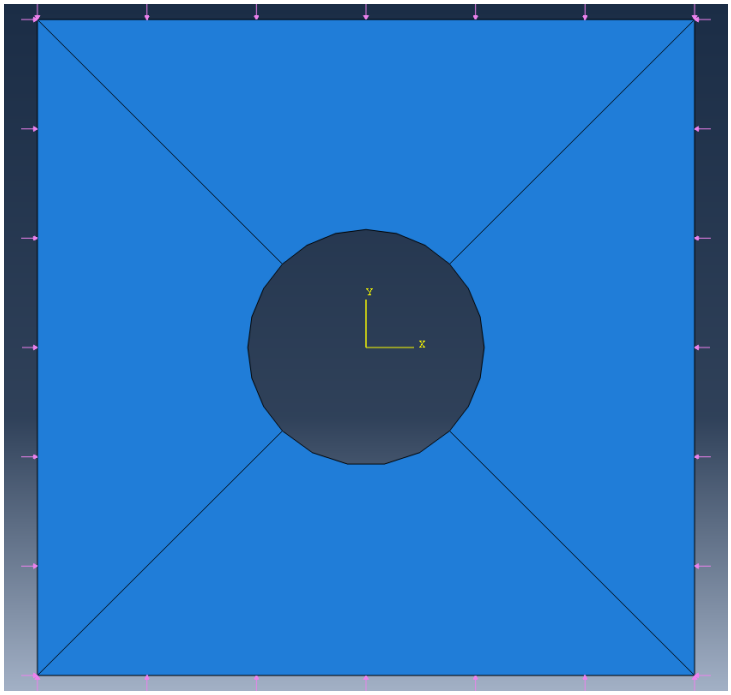

Figure 7-2 Boundary conditions and loads without casing

7.1.1 Elastic stress distribution

The secondary stress field of a bore hole in an infinite elastic half space can be calculated with the classical Kirsch-equation for the simplified case, that the axis of the bore hole is oriented parallel to the principal stress direction. For the general case the bore hole is oriented in any direction in the half space. Here, an analytical solution is also valid. (Compare 4.2)

In order to test the numerical model the equations were compared to the results of the numerical calculations and a good accordance was obtained (Figure 7-3). The dependence of the mesh geometry with regard to the required mesh refinement and the required model size were examined in order to determine mesh dependent calculation results.

7.1.2 Failure criterion

The investigations of rock mechanical questions demonstrated that different criterions of rock failure occurred. The most used one is the Mohr-Coulomb criterion, which was

proved true, although it's simplicity in many cases. A significant characteristic is that the Mohr-Coulomb criterion does not take into account the impact of the mean principle stress of the rock strength.

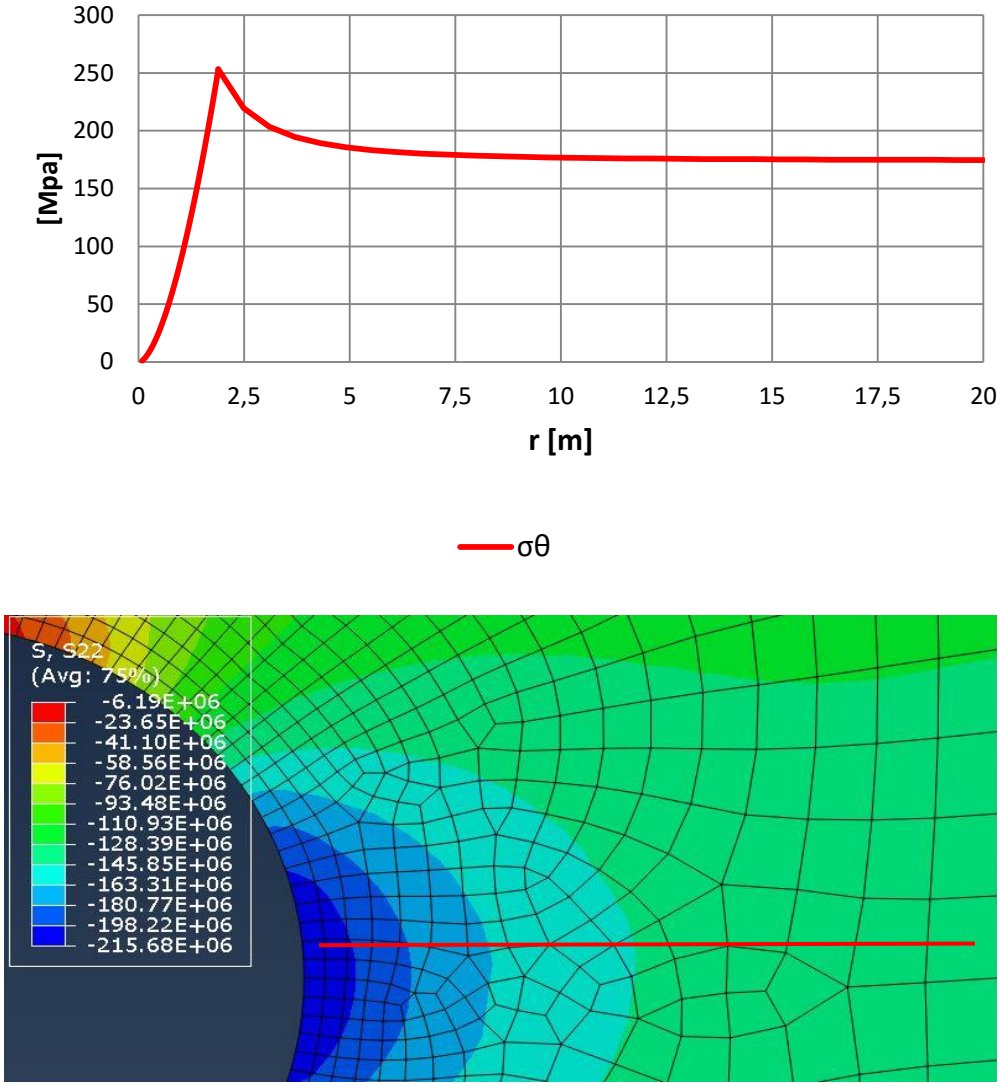

Figure 7-3 Comparison numerical and analytical calculation

7.2 Simulation without bore hole casing

When describing the stress state around a bore hole the diameter of the bore hole is not considered.

In Figure 7-4 is the adjusting effective deviator stress of a bore hole diameter of 7“ at an overburden of 6000 m shown.

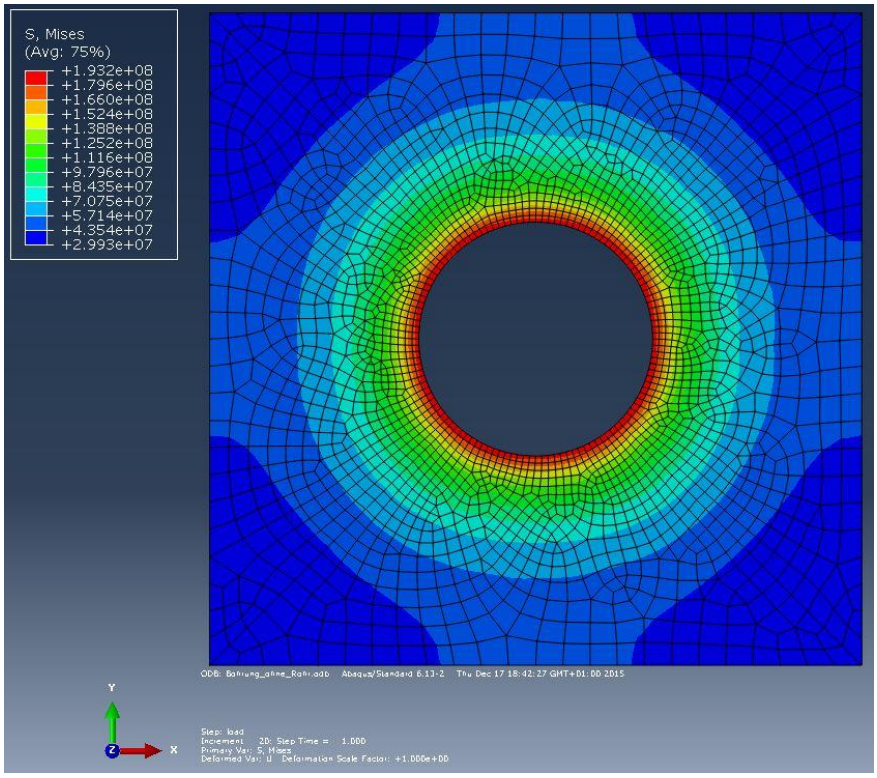

Figure 7-4 Comparative stresses according to v. Mises

The Figure 7-5 and Figure 7-6 show the stress distribution in X and Y direction without casing.

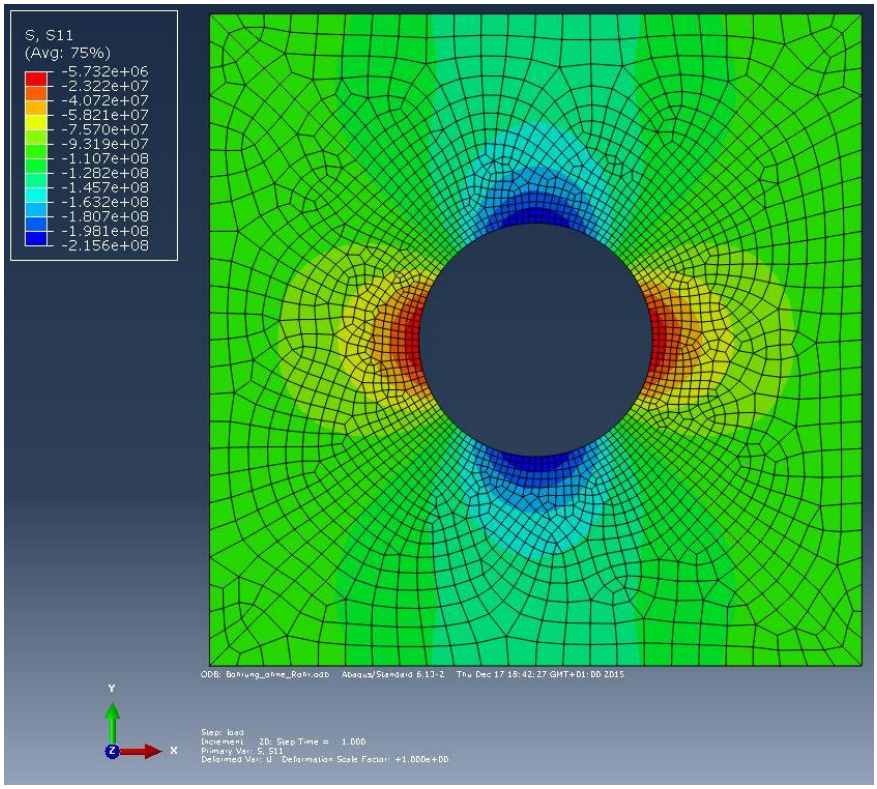

Figure 7-5 Stresses S11 without casing

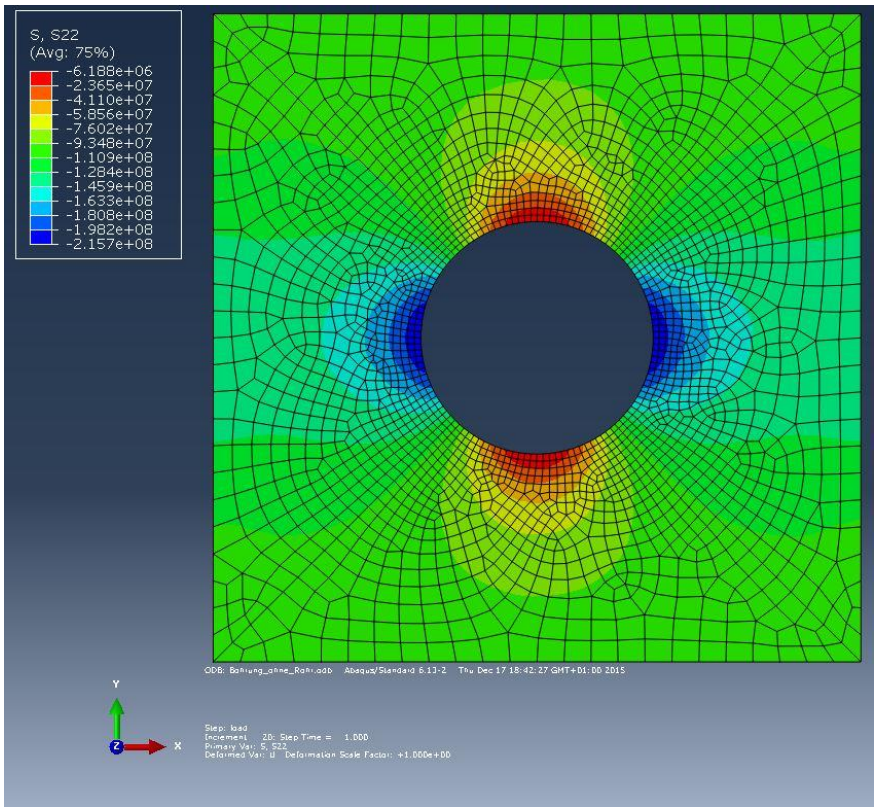

Figure 7-6 Stresses S22 without casing

7.3 Simulation with casing stabilization

To ensure the long-term stability of a deep drilling, the bore hole is piped with casing strings. The casing with a smaller diameter as the one from the bore hole, which is made of steel pipes, is cemented with the rock. So that a hydraulic isolation of the rock is reached and a time dependent destabilization in connection with the inflow of a fluid into the formation is prevented. Furthermore the casing and the cement have a stabilizing impact as support of the bore hole. Also the separation of the different pressure areas of the well and the formation are a required function of the casing.

At the installation of a casing a substantial decrease of the remaining diameter of the drill occurs. That is the reason why the number of used casings is limited and is not able to be built in in any positions wanted.

7.3.1 Numerical model

In Figure 7-7 shown, is a modified finite element model based on the calculations of a cased bore hole section.

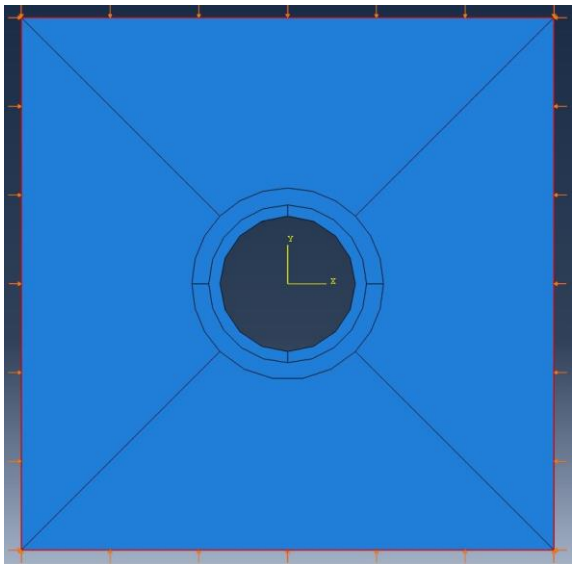

Figure 7-7 Boundary conditions and loads, with casing

The calculation of a cased bore hole is built in three steps. First, the drill is created by removing the elements. Therefore the formation deforms afterwards. This state is equal to the open-hole section, this means the time between the drilling process of the considered section and the cementing of the casing.

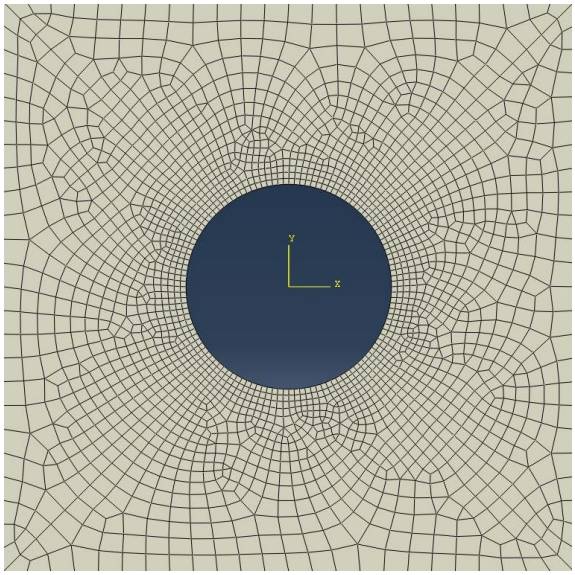

Figure 7-8 Open-hole section

Afterwards the casing is built in and cemented. The influence of the pressure of the cement is not considered in the following model. The cementing occurs in the model abruptly. The cementing of the casing is reached through the reactivation of the before deactivated elements, which represent the concrete and the steel pipe.

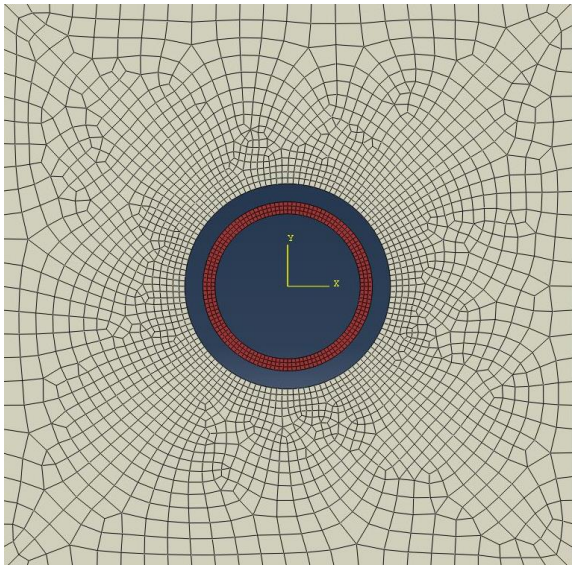

Figure 7-9 Open hole section with casing pipe

Since the steel pipe and the concrete during installation should be tension free, the displacement of the nodes of the cement and the casing were coupled for the duration as open-hole section on the nodes of the bore hole wall. Thus it is

guaranteed that at activation of the elements no sudden displacements occur from prior caused convergence of the bore hole, which could act as additional loads on the concrete and the casing.

7.3.1.1 Parameters of the material

Additionally to the existing model parameters the parameters for the steel pipe as well as the cement are chosen. Since the loads in the steel act within the elastic region, the numerical descriptions could be limited to an elastic model. Plastic deformations do not appear.

Table 7-1 Material parameters for simulation

	Casing pipe T-95	**Cementing**
Youngs modulus	210 000 MPa	40 000 MPa
Poisson ratio	0.3	0.2
density	7800 kg/m³	2500 kg/m³

7.3.1.2 Model

For the considered bore hole a casing with 7" outer diameter is in general used. Typical standardized sizes include wall thicknesses of 12,6 mm (API, 1999). The remaining circle clearance with 19 mm is filled with cement. The steel pipe is discretized with three element rings as well as the cementing. (Figure 7-10)

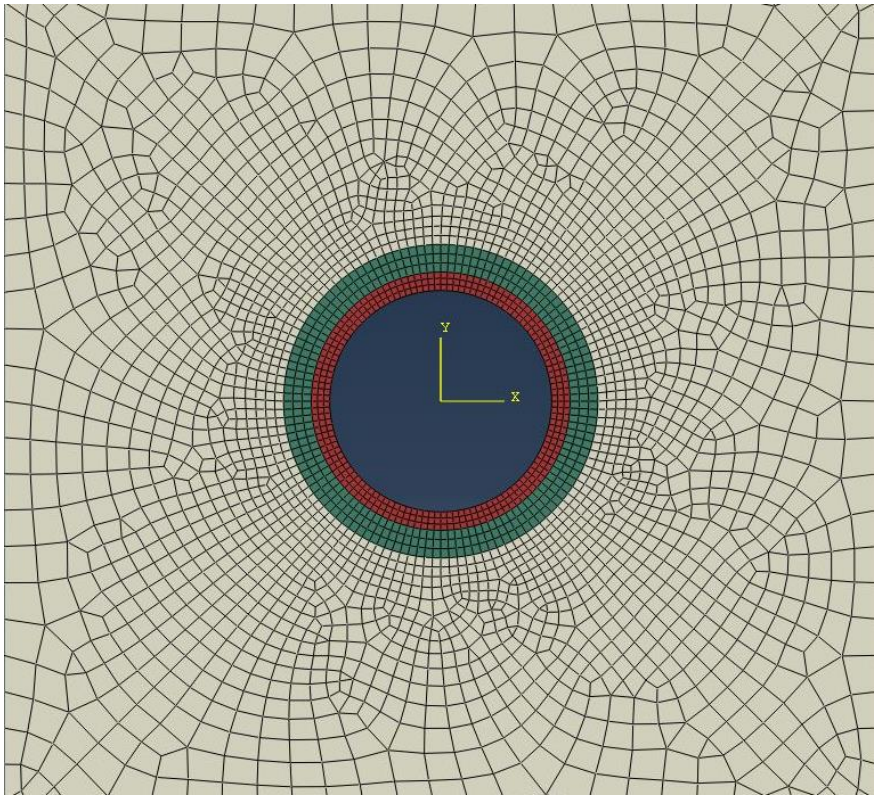

Figure 7-10 Numerical model, casing and cementing

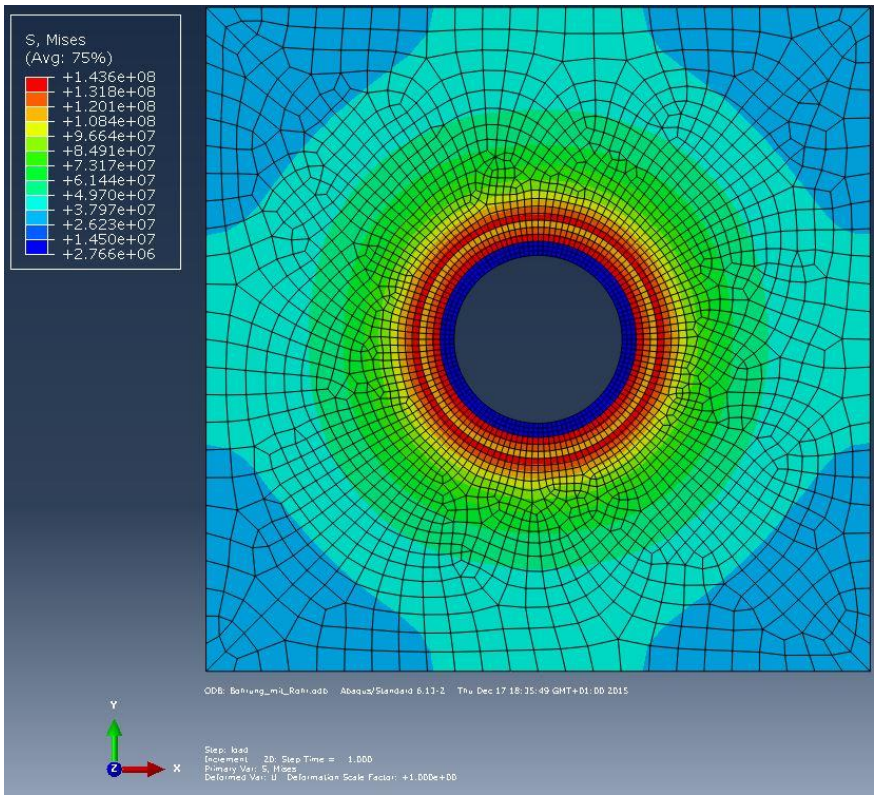

Figure 7-11 Comparative stresses according to v. Mises

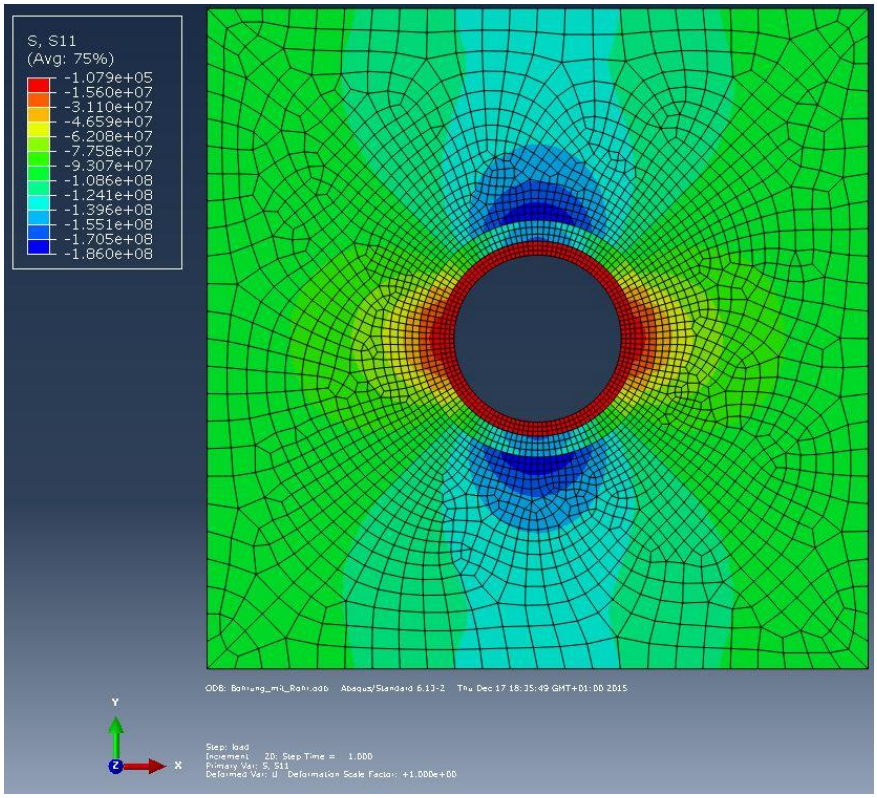

Figure 7-12 Stresses S11, with casing

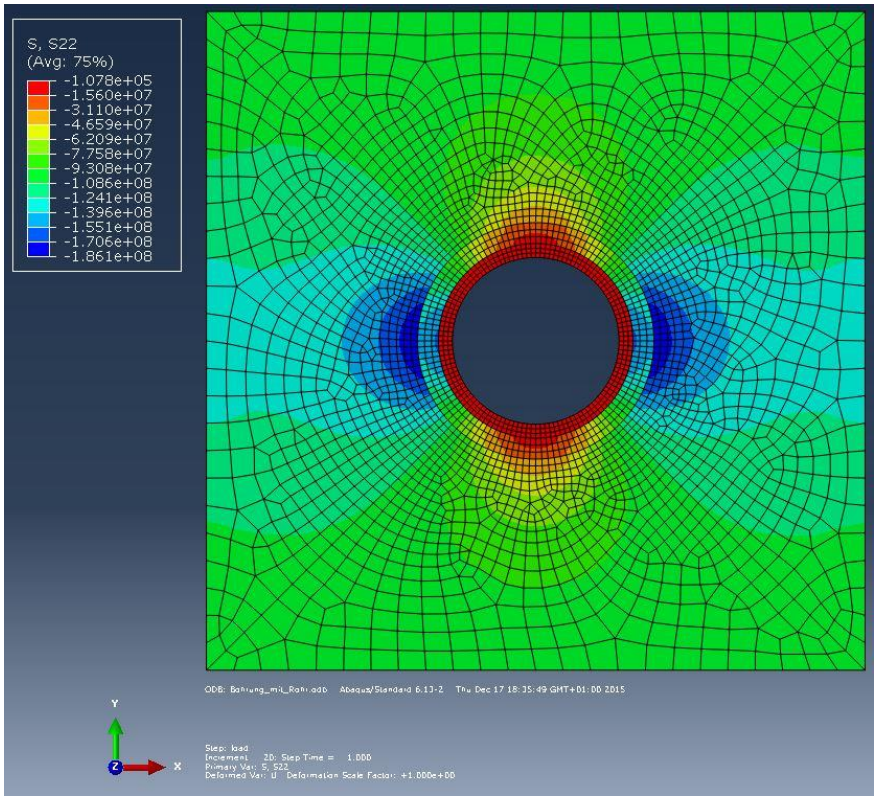

Figure 7-13 Stresses S22, with casing

8 Simulation cavern

The geotechnical importance of petro thermal systems focuses on the stress field in the rocks, which on the one hand naturally exist and on the other hand are changed by the production of subterranean heat exchange areas. When a geothermal thermo well is used, a geotechnical perspective is the stabilization of the bore hole wall by using steel casings. Especially in deeper areas it is significant, because of the rock pressures produced by rising of the overburden. In this case a similar failure mechanism like in the deep shaft construction can occur (rock bursts).

Criteria for selecting a suitable drill rig for drilling in a subsurface structure depend on specific requirements. The excavation of a subsurface cavern, which is suitable for set up a drill rig, is only possible with high technical and time intensive efforts, especially when the excavated material cannot be used as a raw material. In addition the geological and geotechnical conditions must be considered. A drilling rig with the smallest possible base area and height must therefore be prioritized in the selection. To ensure an adequate use of the geothermal temperature at the final depth, the maximum drilling length of the drill rig should not be less than 5000 m. In regard to the power supply must be noted, that the use of diesel- or gas-powered generators for electricity generation can only be used to a certain limit because of the fresh air supply requirements. The potential hazard during ignition or explosion of the used fluids is very high in a closed subsurface structure. Drilling rigs, which are equipped with an external power supply via the power grid, should be preferred.

Following rigs in Central Europe (Germany, Austria) were compared:

- Bauer TBA200 Deep Drilling Unit
- Bauer TBA300 Deep Drilling Unit
- Bentec EURO RIG 350t
- Herrenknecht Vertical Deep Drilling Rig Terra Invader 350 Slingshot
- Herrenknecht Vertical Deep Drilling Rig Terra Invader 350 Box-on-Box
- Max Streicher Tiefbohranlage VDD370
- RAG Energy Drilling Bohranlage E200/E202

Table 8-1 Comparison driiling rigs

	TBA 200 Deep Drilling Unit	TBA 300 Deep Drilling Unit	Bentec Euro Standard Rig 350 t	Herrenknecht Terra Invader 350 Slingshot	Herrenknecht Terra Invader 350 Box-on-Box	Max Streicher VDD370	RAG E200/202
Hook load **Max. hook load**	200 t	300 t	350 t	350 t	350 t	336 t 377 t	250 t 300 t
Max. drilling length	3000 m	5000 m	6000 m	5500 m	5500 m	5000m	5500 m with 3 1/2" DP
Power supply	not specified	or 4x1MW diesel generator	not specified	max. 1540 kVA per generator	max. 1540 kVA per generator	4x852kW AC generator	6x532kW diesel aggregate
via power grid	not specified	20kV	not specified	possible	possible	possible	not specified
Base area	28 m x 30 m 840 m²	23 m x 33 m 759 m²	40 m x 55 m 2200 m²	not specified	not specified	1224 m²	43 m x 85 m 3655 m²
Total height	33 m	41 m	44 m	46 m	52 m	31 m	41 m

A suitable drill rig was determined according to the requirements:

I. Bauer TBA 300 Deep Drilling Unit

The drill rig Bauer TBA 300 Deep Drilling Unit demands the fewest base area, is able to handle the loads and fulfils the drilling requirements. The possibility to supply the drill rig with electrical current is an additional advantage.

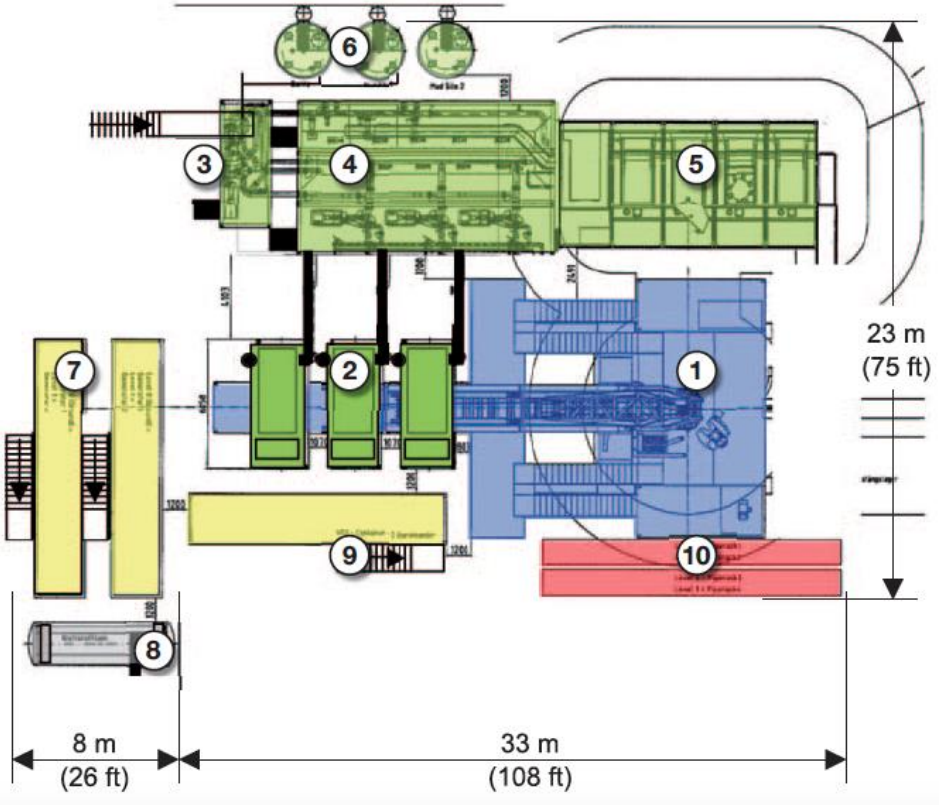

Figure 8-1 Example, base area Bauer TBA 300 Deep Drilling Unit

Considering the given requirements for the cavern diameter a volume of about 72.000 m³ (40 m x 40 m x 45 m) should be provided.

Also a drill set-up area, situated closely to the drilling rig cavern, of about 1.000 m² has to be built. At excavations in that size support requirements are necessary for a stable structure. A support of the cavern is achieved by shotcrete, rock bolts and a two layered reinforcement.

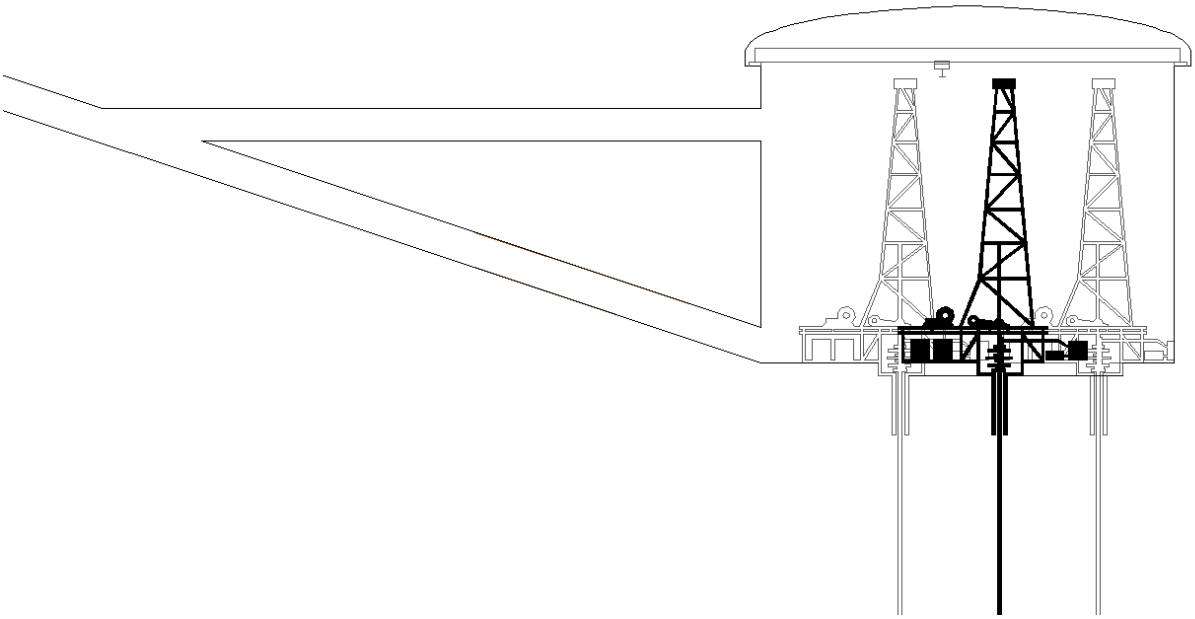

Figure 8-2 Drilling cavern

8.1 Finite element analysis

For the stability analysis of the cavern, which is situated within the deposit in the area of Revier VI/ Mine Breitenau, a finite element analysis was performed. Since not enough parameters were present at this point, they had to be assumed by empirical knowledge. Applying the provided measurement values of the RHI a three dimensional model of a mine structure using a CAD software was simulated. Furthermore a cavern was modeled and integrated into the model. The calculations were made with the finite element program ABAQUS 6.13 CAE, which can determine basic parameters like stress and deformation.

8.1.1 Modeling of a mine structure

Since the original measurement model, which was produced with the software program SUPRAC, contains inaccurate geometries, a revised three dimensional model of the mine and the overlaying rock formations had to be simulated. The inaccurate geometries, which result because of double integration of measurement points, result in further calculations to severe problems when meshing the model in ABAQUS.

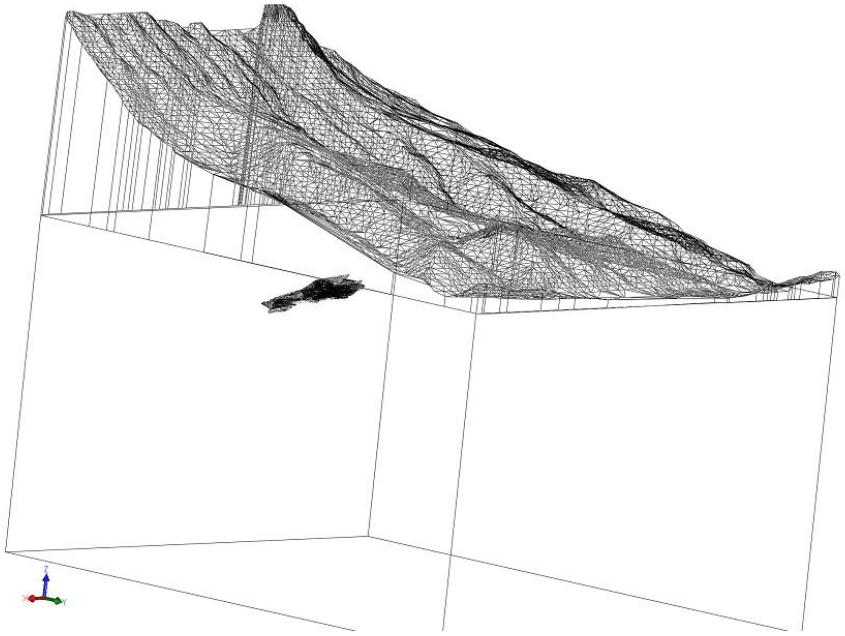

Figure 8-3 Orignal model of mine and surface

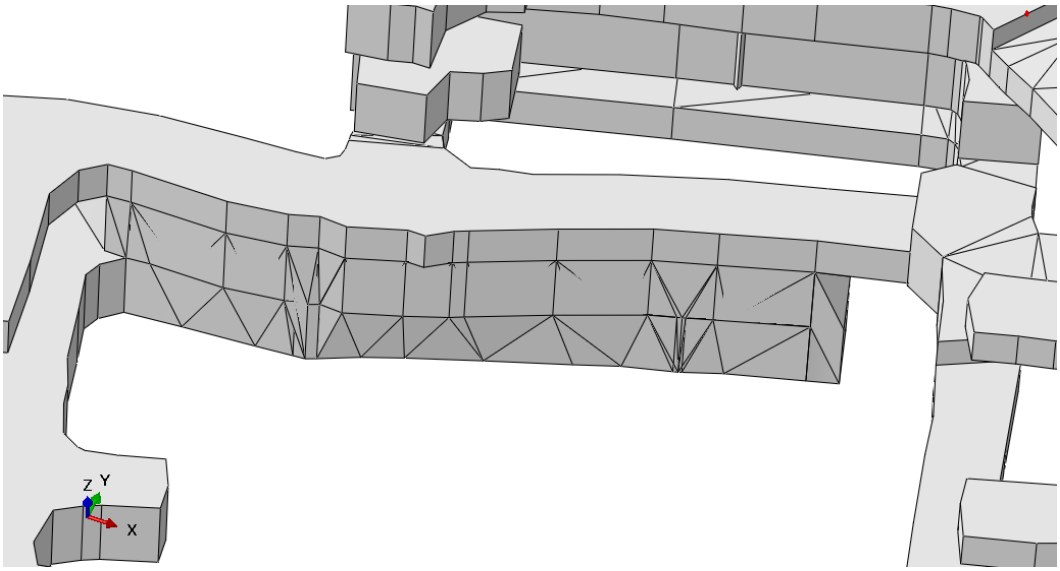

Figure 8-4 Inacurrate geometry

Because the reconstruction the mine structure in a new model, error messages can be eliminated when being meshed The new construction of the model works with the CAD software SOLIDWORKS. Simultaneously the number of distorted elements is reduced, which leads to a rise in mesh quality. Additionally the start cavern and the access tunnel within the deposit are modeled according to predefined dimensions

(compare Figure 8-1) and integrated into the model, in order to be considered in later calculations.

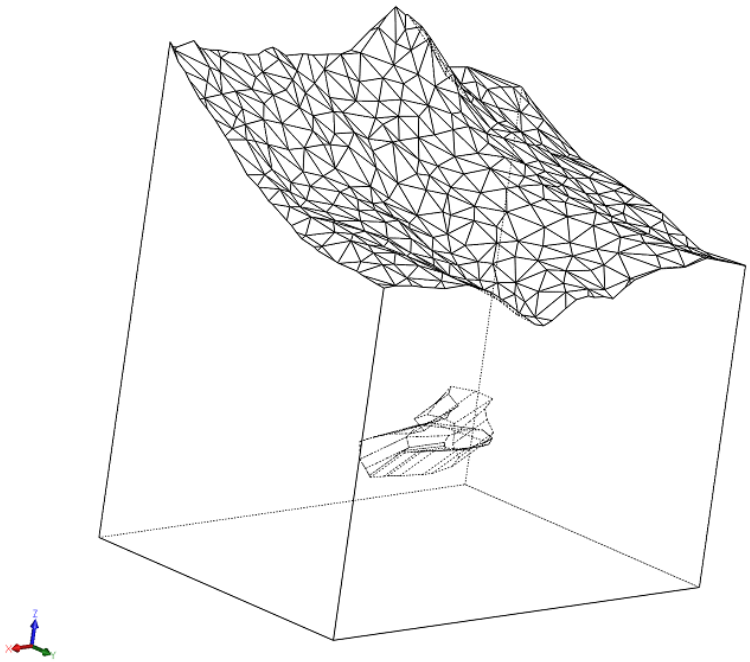

Figure 8-5 New scaled model of the mine, deposit and suface

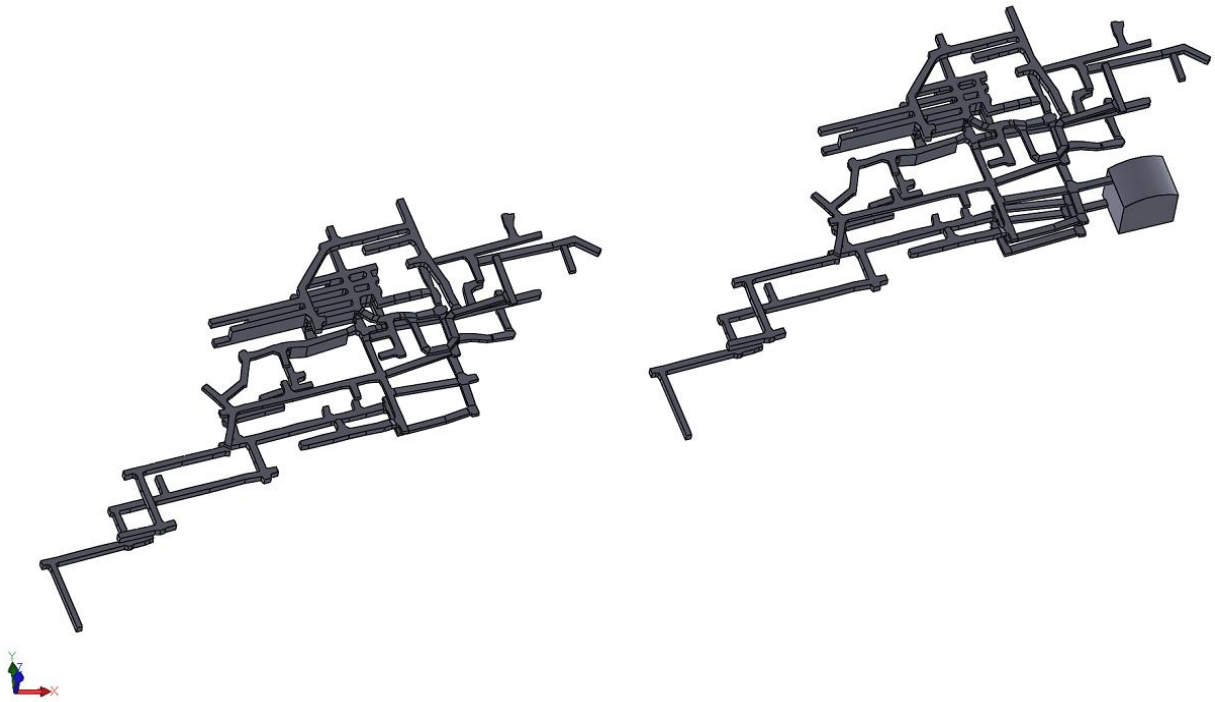

Figure 8-6 New model of mining structure with drilling cavern

8.1.2 Meshing the model

The meshing is performed with the Free Mesh Method because of the complex geometry. Firstly a surface mesh was created from which the volume elements were generated. Furthermore it was necessary to partition the whole area into three sections. The node distances measure on the surface 60 m and decrease towards the mine structure. The areas around the underground structure show with 1-2 m node distance a finer mesh, in order to reach a high accuracy of the stress and displacement distribution.

The whole model consists of more than 5.1 million elements, whereby 500 of them are distorted elements. These elements show an angle of <5° or >170° or a shape factor of <0,001.

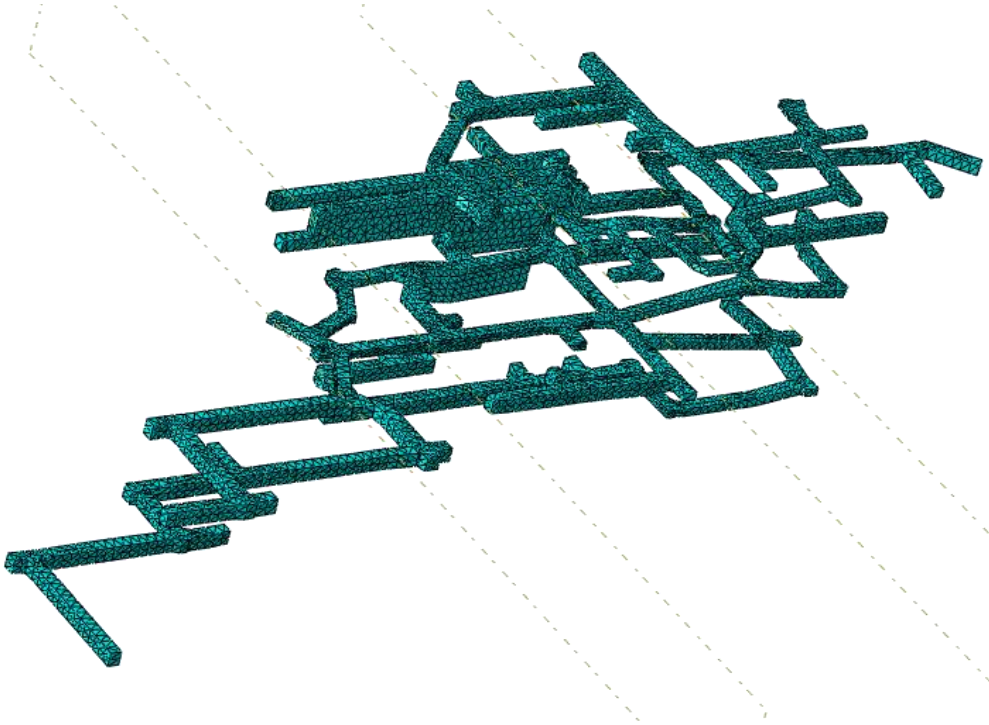

Figure 8-7 Meshed underground structure

The meshing is performed with C3D10 elements (Continuum 3 Dimensonal 10 Node Tetraedal Element). When a complex elasto-plastic material model is used, the elements have to be exchanged by C3D4 elements, since the C3D10 elements would cause long calculation times.

8.1.3 Numerical calculation

The first calculation was performed with a pure elastic material model. This serves mainly the mesh proofing, since for a mesh with poor quality (high number of distorted elements) the calculation process is aborted. In further calculations the mine structure is divided in several layers and the possible positions of the cavern is determined.

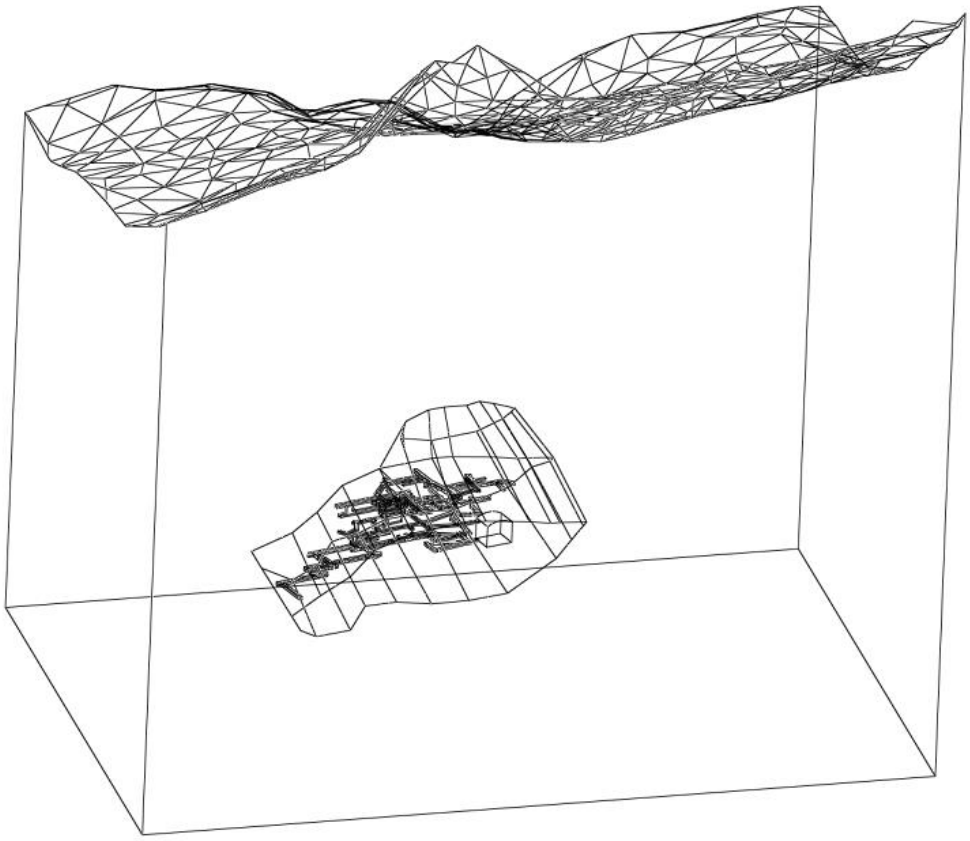

Figure 8-8 Caculation model, mine structure, deposit and surface

8.1.4 Parameters of the material

Since no material parameters of the deposit and the surrounding rock were known at this moment, the calculations had to be performed based on values from the literature.

Table 8-2 Rock parameter

Rock type	density	Young's-modulus	Poisson ratio
	[kg/m^3]	[GPa]	[-]
Lime stone	2700	30	0,3
Magnesite	3100	18	0,25

8.1.5 Calculation steps

The calculation was performed in three steps, which are demonstrated in the following table. The load, which is applied by the volume force, results from the density and the gravity, is performed in step 1. The excavation of the mine structure is included in step 2 with Modell Change.

Table 8-3 Calculation steps

Step	Action	Procedure
Initial	-	
Step1	applying load	Geostatic
Step2	excavation	Static general

8.1.6 Results of the elastic simulation

The results of the numerical simulation submit a primary stress state in a depth of 800 m and 21,64 MPa. The analytical method provides a value for the primary stress of 21,6 MPa. Thus the numerical calculation has a sufficient good approximation. Figure 8-9 shows a section through the surface model using the calculated vertical stresses.

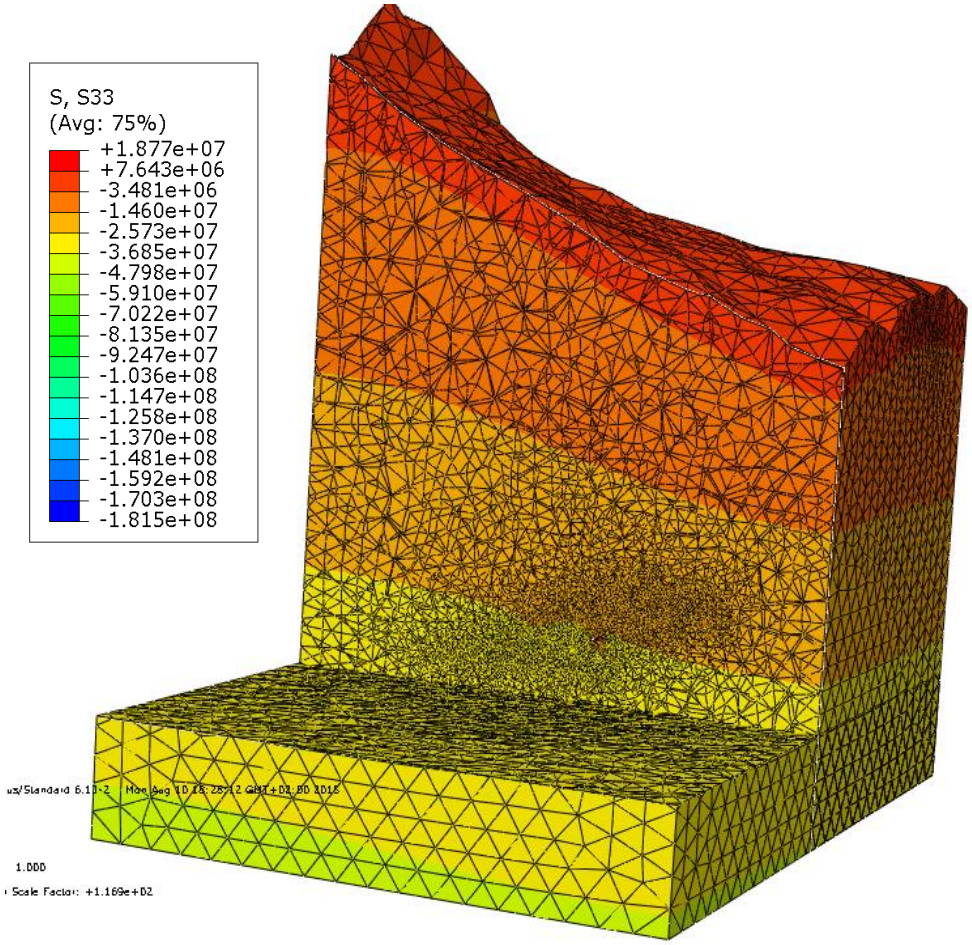

Figure 8-9 Vertical stresses

When an excavation of a mine structure occurs, the primary stresses change around the cavern (induced stresses). A rise of vertical stresses in the area of the sidewall emerges. In the area around the roof and the bottom tensions stresses appear. Thus the numerical simulation provides the same results as the analytical procedures.

Figure 8-10 - Figure 8-12 shows the stress distribution in the area of the excavation chamber. The elevated pressure stresses are presented in the colours yellow and green. The tension stresses in the area of the roof are displayed in red. The numerical calculation provides a first estimation of the stress field in the area of the mining section VI. For the question concerning the whole mining area further calculations with a higher ordered material law have to be performed.

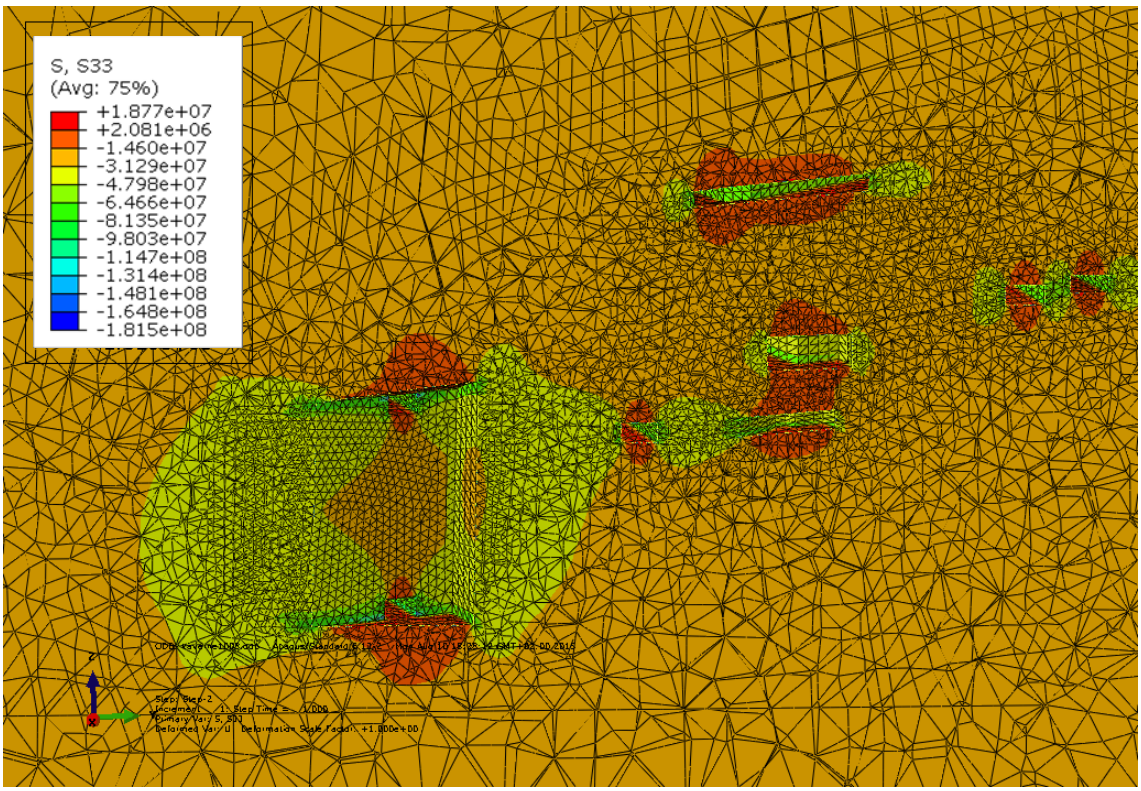

Figure 8-10 Vertical tress distribution arround the drilling cavern, x-x plane

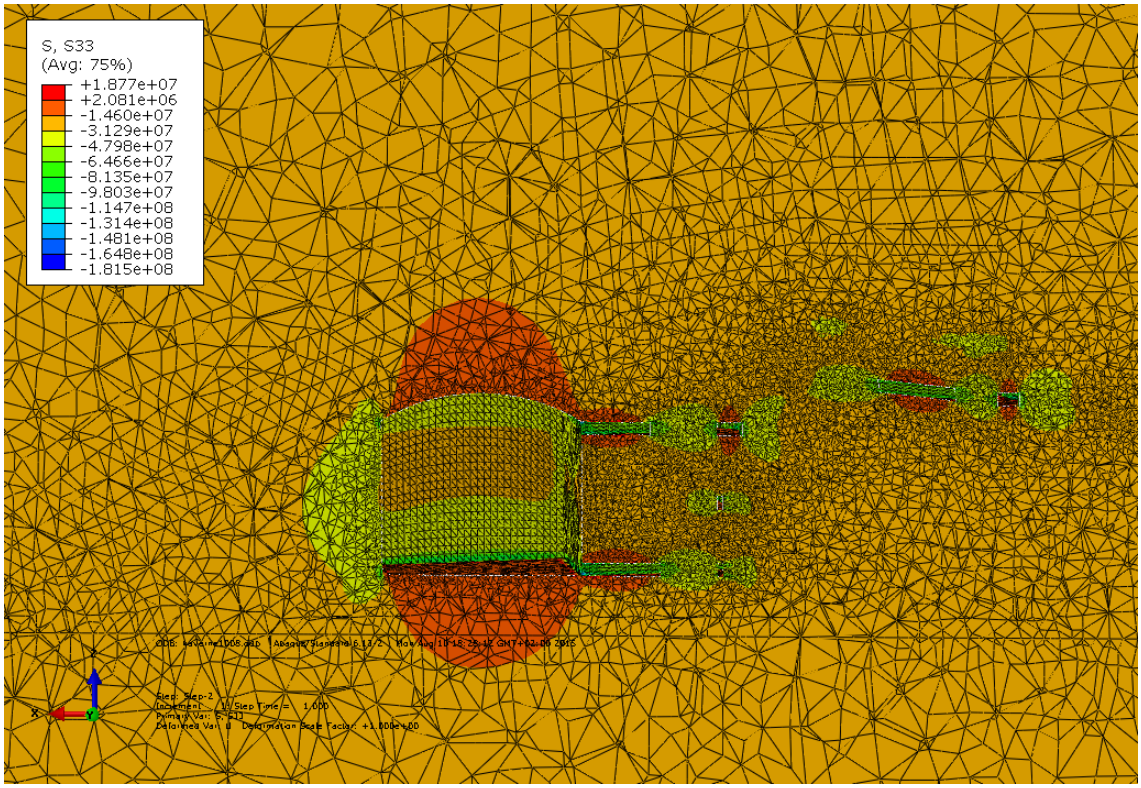

Figure 8-11 Vertical stress distribution arround the drilling cavern, y-y plane

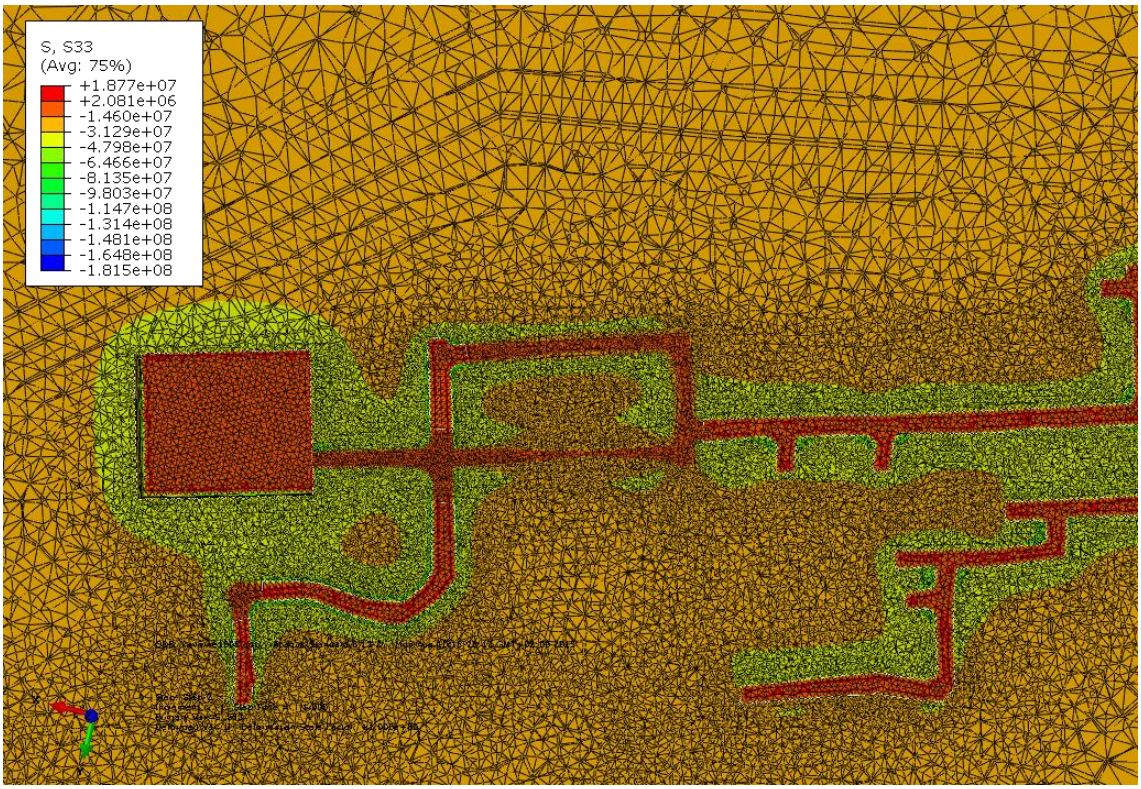

Figure 8-12 Vertical stress distribution arround the drilling cavern and access tunnel, sectional view

9 List of references

API Bulletin 5C2, Bulletin on Performance Properties of Casing, Tubing and Drill Pipe, 21st Edition, October 1999

Bauer M., Freeden W., Jacobi H., Neu Th., 2014. Handbuch Tiefe Geothermie. Springer Verlag, Berlin Heidelberg.

Bourgoyne A.T.Jr., Millheim K.K., Chenevert M.E., Young F.S. Jr., 1986. Applied Drilling Engineering. Society of Petroleum Engineers, Richardson, TX

Gollner, H. & Zier, C., 1982. Stratigraphic Correlation Forms of the Hochlantsch-facies in the Paleozoic of Graz, Padova: s.n

Lake, L. & Mitchel, R., 2006. In: Petroleum Engineering Handbook – Volume II Drilling Engineering.La. s.l.:Society of Petroleum Engineers.

Li G. & Bai M.; Harmonising Rock Engineering and the Environment; 2012, 72 p.

Hood M., and Tutluoglu L., Technologial advances with water jet assisted cutting systems, Lawrence Berkely Laboratory Report to the U.S. Bureau of Mines, 1983

Hubbert, M.K. and Willis, D.G.: "Mechanics of Hydraulic Fracturing," Trans., AIME (1957) 210, 153-160.

Kolymbas D.: Geotechnik – Tunnelbau und Tunnelmechanik; Springer-Verlag Berlin Heidelberg New York; (1998)

Kirsch (1898). “Die Theorie der Elastizität und die Bedürfnisse der Festigkeitslehre”. Zeitschrift des Vereines Deutscher Ingenieure 42, 797–807.

Shuling L., Jeff G., and Cary P. 2012. Pore-Pressure and Wellbore-Stability Prediction to Increase Drilling Efficiency.

RAG, kein Datum Bohranlagen E200/E202-Bohrmannschaft. [Online] Available at: http://www.rag-energy-drilling.at/bohranlagen-e200-e202/personal/bohrmannschaft.html

Veenhuizen, S.D. and T.A. O’Hanlon (1978) “Development of a system for high-speed drilling of smalldiameter roof-bolt holes,” TR117, Water Jet Technology Inc., Kent, Washington.

Vijay M.M., P.E. Grattan-Bellow and W.H. Brierley (1984) “An experimental investigation of drilling and deep slot-ting of hard rocks with rotating high pressure water jets,” Seventh International Symposium on Jet Cutting Technology, Ottowa, Canada, pp. 419-438, BHRA Cranfield, Bedford, England.

Wirtschaftsverband Erdöl-und Erdgasgewinnung, 2006. Leitfaden Futterrohrberechnung. In: s.l.:s.n.

10 List of figures

11 List of tabels

12 Appendix

Table 12-1 stress distribution

stress distribution

	r [m]	σ_θ [Mpa]	σ_R [Mpa]		r [m]	σ_θ [Mpa]	σ_R [Mpa]
PLASTIC ZONE	**0,09**	**1,00**	**0,00**	ELASTISIC ZONE	**1,89**	**253,27**	**94,73**
	0,15	**3,15**	**0,81**		2,50	**219,58**	**128,42**
	0,21	**5,96**	**1,86**		3,10	**203,56**	**144,44**
	0,27	**9,37**	**3,14**		3,70	**194,71**	**153,29**
	0,33	**13,33**	**4,63**		4,31	**189,32**	**158,68**
	0,39	**17,79**	**6,30**		4,91	**185,78**	**162,22**
	0,45	**22,73**	**8,16**		5,51	**183,35**	**164,65**
	0,51	**28,13**	**10,19**		6,12	**181,59**	**166,41**
	0,57	**33,97**	**12,38**		6,72	**180,29**	**167,71**
	0,63	**40,24**	**14,73**		7,33	**179,30**	**168,70**
	0,69	**46,91**	**17,24**		7,93	**178,52**	**169,48**
	0,75	**53,97**	**19,89**		8,53	**177,90**	**170,10**
	0,81	**61,43**	**22,69**		9,14	**177,41**	**170,59**
	0,87	**69,26**	**25,63**		9,74	**177,00**	**171,00**
	0,93	**77,45**	**28,71**		10,34	**176,66**	**171,34**
	0,99	**86,01**	**31,92**		10,95	**176,37**	**171,63**
	1,05	**94,91**	**35,27**		11,55	**176,13**	**171,87**
	1,11	**104,16**	**38,74**		12,15	**175,92**	**172,08**
	1,17	**113,74**	**42,34**		12,76	**175,75**	**172,25**
	1,23	**123,66**	**46,06**		13,36	**175,59**	**172,41**
	1,29	**133,90**	**49,91**		13,96	**175,46**	**172,54**
	1,35	**144,47**	**53,88**		14,57	**175,34**	**172,66**
	1,41	**155,35**	**57,96**		15,17	**175,23**	**172,77**
	1,47	**166,54**	**62,17**		15,78	**175,14**	**172,86**
	1,53	**178,04**	**66,48**		16,38	**175,06**	**172,94**
	1,59	**189,84**	**70,92**		16,98	**174,99**	**173,01**
	1,65	**201,94**	**75,46**		17,59	**174,92**	**173,08**
	1,71	**214,34**	**80,11**		18,19	**174,86**	**173,14**
	1,77	**227,03**	**84,88**		18,79	**174,80**	**173,20**
	1,83	**240,01**	**89,75**		19,40	**174,76**	**173,24**
	1,89	**253,27**	**94,73**		**20,00**	**174,71**	**173,29**

Table 12-2 stress distribution

stress distribution

	r [m]	σ_θ [Mpa]	σ_R [Mpa]		r [m]	σ_θ [Mpa]	σ_R [Mpa]
PLASTIC ZONE	**0,13**	**1,00**	**0,00**	ELASTISIC ZONE	**1,90**	**147,85**	**55,15**
	0,18	**2,45**	**0,55**		2,51	**128,24**	**74,76**
	0,24	**4,26**	**1,22**		3,11	**118,87**	**84,13**
	0,30	**6,38**	**2,02**		3,71	**113,69**	**89,31**
	0,36	**8,80**	**2,93**		4,32	**110,52**	**92,48**
	0,42	**11,49**	**3,94**		4,92	**108,45**	**94,55**
	0,48	**14,45**	**5,05**		5,52	**107,01**	**95,99**
	0,54	**17,66**	**6,26**		6,13	**105,98**	**97,02**
	0,60	**21,12**	**7,55**		6,73	**105,21**	**97,79**
	0,66	**24,81**	**8,94**		7,33	**104,63**	**98,37**
	0,72	**28,72**	**10,41**		7,94	**104,17**	**98,83**
	0,78	**32,86**	**11,96**		8,54	**103,81**	**99,19**
	0,84	**37,21**	**13,60**		9,14	**103,51**	**99,49**
	0,90	**41,77**	**15,31**		9,75	**103,27**	**99,73**
	0,96	**46,54**	**17,10**		10,35	**103,07**	**99,93**
	1,01	**51,51**	**18,97**		10,95	**102,90**	**100,10**
	1,07	**56,67**	**20,91**		11,56	**102,76**	**100,24**
	1,13	**62,02**	**22,92**		12,16	**102,64**	**100,36**
	1,19	**67,57**	**25,00**		12,76	**102,53**	**100,47**
	1,25	**73,30**	**27,15**		13,37	**102,44**	**100,56**
	1,31	**79,21**	**29,37**		13,97	**102,36**	**100,64**
	1,37	**85,31**	**31,66**		14,57	**102,29**	**100,71**
	1,43	**91,58**	**34,01**		15,17	**102,23**	**100,77**
	1,49	**98,02**	**36,43**		15,78	**102,18**	**100,82**
	1,55	**104,64**	**38,92**		16,38	**102,13**	**100,87**
	1,61	**111,43**	**41,47**		16,98	**102,08**	**100,92**
	1,67	**118,39**	**44,08**		17,59	**102,04**	**100,96**
	1,73	**125,51**	**46,76**		18,19	**102,01**	**100,99**
	1,79	**132,79**	**49,49**		18,79	**101,98**	**101,02**
	1,85	**140,24**	**52,29**		19,40	**101,95**	**101,05**
	1,90	**147,85**	**55,15**		**20,00**	**101,92**	**101,08**

Table 12-3 Calculation case A

Casing Ratings, Worst Case kick from next section @ surface, intermediate / leaky tubing @ production						
Section	**Surface**		**Intermediate**		**Production**	
	[bar]	**[psi]**	**[bar]**	**[psi]**	**[bar]**	**[psi]**
Hydrostatic mud	124	1795	346	5019	599	8683
Collapse design load	139	2020	389	5647	674	9769
Burst design load	370	5360	639	9273	639	9273
Select Casing						
Quality	**C-90**	**13 3/8" 68lb/f**	**T-95**	**9 5/8" 53.5 lb**	**T-95**	**7" 35 lb/ft**
OD	13 3/8	in	9 5/8	in	7	in
ID	12,415	in	8,535	in	6,004	in
Weight	101,20	kg/m	79,62	kg/m	52,09	kg/m
Coupling	STC		LTC		LTC	
Collapse resistance	2320	psi	7340	psi	11650	psi
	160	bar	506	bar	803	bar
Burst resistance	5650	psi	9410	psi	10970	psi
	390	bar	649	bar	756	bar
Yield Strength	1057	1000 lbs	1220	1000 lbs	853	1000 lbs
	4702	kN	5427	kN	3794	kN
Design on Collapse						
Load	139	bar	389	bar	674	bar
Back load	0	bar	0	bar	0	bar
Safety Factor	**1,15**		**1,30**		**1,19**	
Design on Burst						
Load	336	bar	581	bar	581	bar
Back load	0	bar	0	bar	0	bar
Safety Factor	**1,16**		**1,12**		**1,30**	
Design on Tension						
Load	123 966	kg	272 691	kg	135 425	kg
BF	1,000	(in air)	1,000	(in air)	1,000	(in air)
Load*F	123 966	kg	272 691	kg	135 425	kg
Safety Factor	**3,87**		**2,03**		**2,86**	

Casing Ratings, Realistic Case kick from next section @ surface, intermediate / leaky tubing @ production						
Section	**Surface**		**Intermediate**		**Production**	
	[bar]	**[psi]**	**[bar]**	**[psi]**	**[bar]**	**[psi]**
Hydrostatic mud	124	1795	346	5019	599	8683
Collapse design load	139	2020	389	5647	674	9769
Burst design load	253	3672	708	10267	639	9273
Select Casing						
Quality	**C-90**	**13 3/8" 68 lb/**	**S-95**	**9 5/8" 53.5 lb**	**T-95**	**7" 35 lb/ft**
OD	13 3/8	in	9 5/8	in	7	in
ID	12,415	in	8,535	in	6,004	in
Weight	101,20	kg/m	79,62	kg/m	52,09	kg/m
Coupling	STC		LTC		LTC	
Collapse resistance	2320	psi	8850	psi	11650	psi
	160	bar	610	bar	803	bar
Burst resistance	5650	psi	9410	psi	10970	psi
	390	bar	649	bar	756	bar
Yield Strength	1057	1000 lbs	1235	1000 lbs	853	1000 lbs
	4702	kN	5493	kN	3794	kN
Design on Collapse						
Load	139	bar	389	bar	674	bar
Back load	0	bar	0	bar	0	bar
Safety Factor	**1,15**		**1,57**		**1,19**	
Design on Burst						
Load	230	bar	644	bar	581	bar
Back load	0	bar	0	bar	0	bar
Safety Factor	**1,69**		**1,01**		**1,30**	
Design on Tension						
Load	123 966	kg	272 691	kg	135 425	kg
BF	0,869		0,869		0,869	
Load*F	107 700	kg	236 911	kg	117 656	kg
Safety Factor	**4,45**		**2,36**		**3,29**	